Available online at www.sciencedirect.com

SciVerse ScienceDirect

journal homepage: www.elsevier.com/locate/jmbbm

Research paper

A mesostructurally-based anisotropic continuum model for biological soft tissues—Decoupled invariant formulation

*Georges Limbert**

National Centre for Advanced Tribology at Southampton (nCATS), Faculty of Engineering and the Environment, University of Southampton, Southampton SO17 1BJ, United Kingdom

Bioengineering Science Research Group, Faculty of Engineering and the Environment, University of Southampton, Southampton SO17 1BJ, United Kingdom

ARTICLE INFO

Article history:
Published online 2 August 2011

Keywords:
Soft tissue
Constitutive model
Anisotropic hyperelasticity
Entropic elasticity
Tropocollagen
Collagen
Multi-scale modelling
Skin

ABSTRACT

Characterising and modelling the mechanical behaviour of biological soft tissues is an essential step in the development of predictive computational models to assist research for a wide range of applications in medicine, biology, tissue engineering, pharmaceutics, consumer goods, cosmetics, transport or military. It is therefore critical to develop constitutive models that can capture particular rheological mechanisms operating at specific length scales so that these models are adapted for their intended applications.

Here, a novel mesoscopically-based decoupled invariant-based continuum constitutive framework for transversely isotropic and orthotropic biological soft tissues is developed. A notable feature of the formulation is the full decoupling of shear interactions. The constitutive model is based on a combination of the framework proposed by Lu and Zhang [Lu, J., Zhang, L., 2005. Physically motivated invariant formulation for transversely isotropic hyperelasticity. International Journal of Solids and Structures 42, 6015–6031] and the entropic mechanics of tropocollagen molecules and collagen assemblies. One of the key aspects of the formulation is to use physically-based nanoscopic quantities that could be extracted from experiments and/or atomistic/molecular dynamics simulations to inform the macroscopic constitutive behaviour. This effectively couples the material properties at different levels of the multi-scale hierarchical structure of collagenous tissues. The orthotropic hyperelastic model was shown to reproduce very well the experimental multi-axial properties of rabbit skin. A new insight into the shear response of a skin sample subjected to a simulated indentation test was obtained using numerical direct sensitivity analyses.

1. Introduction

Characterising and predicting the mechanical behaviour of biological soft tissues is an essential requirement for conducting computer experiments using finite element or computational fluid dynamics techniques. The domains of application have expanded well beyond medicine and automotive safety to reach other fields such as consumer products, cosmetics (Limbert, 2009), sports equipment or computer graphics. It is therefore critical to develop

* Correspondence to: National Centre for Advanced Tribology at Southampton (nCATS), Faculty of Engineering and the Environment, University of Southampton, Southampton SO17 1BJ, United Kingdom.
E-mail address: g.limbert@soton.ac.uk.

1751-6161/$ - see front matter © 2011 Elsevier Ltd. All rights reserved.
doi:10.1016/j.jmbbm.2011.07.016

constitutive models that can capture particular mechanical features operating at specific length scales so that these models are adapted for their intended applications. Besides their living nature, the main characteristics of biological soft connective tissues is that they can sustain large deformations under physiological or abnormal conditions, have a highly nonlinear behaviour and possess strongly anisotropic mechanical properties (Fung, 1981).

The complex multi-scale hierarchical nature of biological tissues and the associated challenges in their bottom-up experimental characterisation have limited the development of structural models (Hurschler et al., 1997) in favour of continuum-based models. This latter class of models can provide a very good approximation of the macroscopic mechanics of soft tissue structures such as ligaments (Limbert et al., 2003, 2004; Pioletti et al., 1998; Weiss et al., 1996), tendons (Pioletti et al., 1998), arteries (Holzapfel et al., 2000; Humphrey and Yin, 1987) or skin (Bischoff et al., 2002a,b; Lanir, 1983; Oomens et al., 1987).

The traditional approach to formulate constitutive laws for biological soft tissues has been mainly based on invariant formulations which postulate the existence of a strain energy function depending on a set of tensorial invariants of a given deformation or strain measure. The key element in these procedures is to select a set of tensor invariants that characterise the particular deformation modes the tissue is known to be subjected to and that have also a physical interpretation so that constitutive parameters can be directly related to experimental measurements. For collagen fibre-rich tissues, a classic assumption is to consider the tissue as a composite material made of one or several families of (oriented) collagen fibres embedded in a highly compliant isotropic solid matrix composed mainly of proteoglycans. The preferred fibre alignment is defined by the introduction of a so-called structural tensor which appears as an argument of the strain energy function (Boehler, 1978; Spencer, 1992a). Generally, a principle of linear superposition of the fibre and matrix strain energies is also assumed (Holzapfel et al., 2000; Humphrey, 2003; Humphrey and Yin, 1987; Limbert and Taylor, 2002; Weiss et al., 1996) but, for most studies, and by construction, fails to account for the fibre–fibre and fibre–matrix interactions which can be highly relevant in certain conditions (e.g. warping and sliding of the knee cruciate ligaments). To date, only few studies have integrated these shear interactions into constitutive formulations (Blemker et al., 2005; Guo et al., 2006; Ito et al., 2010; Peng et al., 2006; Tang et al., 2009, 2010; Wagner and Lotz, 2004).

In the last decade, the terrific advances in atomistic and molecular modelling techniques – and more generally multi-scale modelling techniques (Buehler, 2006a,b, 2008c; Buehler and Wong, 2007; Gautieri et al., 2009a, 2010; Tang et al., 2009) – have permitted to overcome some of the challenges posed by the bottom-up experimental characterisation of collagenous tissues. Novel insights into the hierarchical deformation and fracture mechanisms have been made possible and have helped to deepen our current understanding of the multi-scale behaviour of biological soft tissues. The information obtained from these multi-scale modelling simulations, together with corroborated experimental data (Fratzl, 2008) are essential in the development of nano/micro-structurally-based macroscopic continuum models. In a recent study, Tang et al. (2009) embraced this paradigm by proposing a pioneering continuum constitutive model of collagenous soft tissues integrating explicit nanoscopic structural and material properties into the formulation. The basis for the formulation was to introduce a multiplicative decomposition of the macroscopic deformation gradient into a pure uniaxial deformation along the fibre direction and a deformation containing shear and rigid body rotations. This macroscopic deformation gradient, defined at each material point, was assumed to be a volume average of the deformation gradient operating at the lower level of the tissue structural hierarchy, that is, the scale of individual fibrils. The (finite strain) mechanical behaviour of the fibrils was assumed to be elastoplastic. The local mesoscopic deformation gradient controlling the deformation of fibrils was kinematically decomposed into an elastic and a plastic component. In their constitutive formulation Tang et al. (2009) linked the macroscopic tensile properties of the tissue with a parameter representing the relative strength of the intermolecular adhesion with respect to a reference value corresponding to non-covalent intermolecular interactions (Buehler, 2008d). This ratio parameter was effectively controlling the yield strength of fibrils. The shear modulus of individual fibrils, the critical stretch at which fibrils enter a secondary deformation regime (plastic flow) and the exponent parameter of the plastic flow evolution function were estimated by fitting the continuum response of a fibril to the results obtained from molecular dynamics simulations. The transversely isotropic multi-scale model was shown to capture the typical mechanical response of soft tissues: toe region, stiffening and then softening before ultimate rupture. However, the individual phases of the constitutive formulation (fibrils, fibres and matrix materials) were all assumed to be incompressible and there was no full decoupling between the shear, volumetric and along the fibre deformation modes.

Criscione et al. (2001) first proposed a set of five strain invariants that capture distinct kinematic modes of deformation – pure dilatation, the distortional stretch in the fibre direction, two shear modes and their relative orientations – for transversely isotropic hyperelastic solids. This effectively leads to a five-terms decoupled representation of the stress tensors. Each of these terms are *mostly* orthogonal to each others. The motivation behind these invariants was to establish a framework to link directly experimental measurements to the constitutive parameters of the strain energy function describing the mechanics of biological soft tissues. The derivation of Criscione et al. (2001) was later extended to laminar materials with one family of fibres (Criscione et al., 2002) and general anisotropic hyperelastic solids with two families of fibre (Criscione and Hunter, 2003). A drawback of the formulation lies in its inability to obtain fully orthogonal stress terms and the use of transcendental functions to define the kinematic invariants. This shortcoming was later addressed by Lu and Zhang (2005) who proposed a kinetic split of the Cauchy stress tensor into pure hydrostatic pressure, deviatoric fibre tension, transverse (along-fibre) and in-plane (cross-fibre) shear stress for transversely isotropic hyperelastic

materials. These authors established a multiplicative decomposition of the deformation gradient into a pure volumetric term, a deviatoric fibre stretch and a term corresponding to a volume-preserving deformation followed by a compression along the fibre direction such that the deviatoric fibre stretch is unity. The fictitious Cauchy stress resulting from this latter modified deformation gradient was shown to be work-conjugate to the transverse and in-plane shear stress. To model the intra-lamellar fibre–fibre interactions of the annulus fibrosus Wagner and Lotz (2004) used a strain energy term combining the two transversely isotropic invariants I_4 and I_5 of the Spencer theory (to be described in more details in Section 2). The constitutive framework of Criscione et al. (2001) was exploited by Blemker et al. (2005) in the development of a three-dimensional constitutive model of the biceps brachii. They accounted for transverse and in-plane shear stress by using a strain energy function featuring quadratic terms in the shear invariants established by Criscione et al. (2001). Results demonstrated the significant influence of the transverse shear stress on the mechanical response of the muscle and hence, the usefulness of the novel decoupled representation of the deformation. A similar approach was recently adopted by Ito et al. (2010) for the formulation of a constitutive model of skeletal muscle accounting for anisotropic damage. Using kinematic arguments considering the angle between the deformed fibre vector and the vector normal to the deformed differential area element Peng et al. (2006) devised a new invariant characterising the fibre–matrix and fibre–fibre shear interaction energy. Borrowing ideas on shear tensorial invariants from Peng et al. (2006), Guo et al. (2006) developed a composite-based orthotropic hyperelastic constitutive model of the annulus fibrosus capturing the matrix–fibre shear energy. These latter authors demonstrated a good agreement between their and Peng et al.'s model and the ability of both models to represent the observed behaviour of the annulus fibrosus (Bass et al., 2004).

The objective of the present study is two-fold. The first one is to develop a *fully* decoupled invariant-based continuum constitutive framework for transversely isotropic hyperelastic soft tissues. This will be achieved by combining the invariant formulation proposed by Lu and Zhang (2005) to the entropic mechanics of tropocollagen molecules. One of the key elements of the formulation is to use physically-based nanoscopic quantities that could be extracted from experiments and/or atomistic/molecular dynamics simulations to inform the macroscopic constitutive behaviour. This effectively couples the material properties at different levels of the multi-scale hierarchical structure of collagenous tissues. The transversely isotropic framework will be extended to orthotropic symmetry by including an additional family of oriented fibres (Holzapfel, 2000; Limbert and Taylor, 2002; Spencer, 1992a). The second objective is to test the ability of the constitutive model to capture the experimental multi-directional mechanics of rabbit skin (Lanir and Fung, 1972) and to assess some of its mechanical characteristics, and more particularly with regards to shear deformations.

Section 2 presents the constitutive framework for the decoupled invariant formulation while particularisation of the strain energy functional form for biological soft tissues with transverse isotropic and orthotropic symmetries is established in Section 3. The methodology to identify the constitutive parameters of the model with experimental data is presented in Section 4. Parametric and sensitivity analyses of the orthotropic hyperelastic constitutive model are described in Section 5. Finally Sections 6 and 7 contain results, discussion and conclusion to the study.

2. Constitutive formulation

2.1. *Finite kinematics of a transversely isotropic solid*

Let us consider a body $\mathcal{B}$ of the three-dimensional Euclidean space in its reference configuration Ω_0. Following standard usage in continuum mechanics, we denote by $\mathbf{X}$ and $\mathbf{x}$ the position of an arbitrary material point of $\mathcal{B}$ in respectively the reference and current configurations Ω_0 and Ω. The objective function $\varphi : \Omega_0 \rightarrow \Omega$ mapping $\mathbf{X}$ to $\mathbf{x} = \varphi(\mathbf{X})$ is the deformation. The deformation gradient is then defined as $\mathbf{F}(\mathbf{X}) = \partial\varphi(\mathbf{X})/\partial\mathbf{X} = \partial\mathbf{x}/\partial\mathbf{X}$ and the Jacobian of the deformation is $J = \det(\mathbf{F})$. Without loss of generality, it is assumed here that the kinematics of $\mathcal{B}$ is described using orthonormal bases in the Lagrangian and Eulerian configurations so that the two metric tensors reduce to the second-order identity tensor $\mathbf{I}$. The right and left Cauchy–Green deformation tensors are respectively defined as $\mathbf{C} = \mathbf{F}^{\mathrm{T}}\mathbf{F}$ and $\mathbf{b} = \mathbf{F}\mathbf{F}^{\mathrm{T}}$ where the superscript "T" denotes the transpose of a tensor. For subsequent developments, one also defines "$\otimes$" as the outer tensor product operator, ":" as the double contracted tensor product operator and trace($\bullet$) as the trace of a tensor $\bullet$.

The simplest case of anisotropic material is represented by an isotropic solid matrix containing one family of fibres possessing a single preferred principal direction (at least, locally). This represents *transversely isotropic* symmetry. Any orthogonal transformation member of the symmetry group of the material must leave the strain energy function unchanged when applied to the material in the natural state (prior to deformation) (Ogden, 1984). If $\boldsymbol{n}_0 = \boldsymbol{n}_0(\mathbf{X})$ represents the unit vector tangent to the local fibre orientation in the reference configuration, a set of five scalar-valued tensor invariants $\{I_i\}_{i=1,\ldots,5}$ is necessary to form the *irreducible integrity bases* of the tensors $\mathbf{C}$ and $\boldsymbol{\Lambda}_0 = \boldsymbol{n}_0 \otimes \boldsymbol{n}_0$ (Boehler, 1978; Spencer, 1992a). This means that there must exist a strain energy function $\Psi = \Psi(I_1, I_2, I_3, I_4, I_5)$ where the classical principal invariants of $\mathbf{C}$ are given by:

$$I_1 = \mathrm{trace}(\mathbf{C}), \qquad I_2 = \frac{1}{2}[I_1 - \mathrm{trace}(\mathbf{C}^2)], \qquad I_3 = \det(\mathbf{C}) \tag{1}$$

and are augmented with anisotropic invariants I_4 and I_5 depending on $\mathbf{C}$ and the material structural tensor $\boldsymbol{\Lambda}_0$:

$$I_4 = \mathbf{C} : \boldsymbol{\Lambda}_0, \qquad I_5 = \mathbf{C}^2 : \boldsymbol{\Lambda}_0. \tag{2}$$

If λ denotes the stretch in the fibre direction $\boldsymbol{n}_0$ defined by $\mathbf{F}\boldsymbol{n}_0 = \lambda\boldsymbol{n} - \boldsymbol{n}$ being the unit vector tangent to the fibre direction in the deformed configuration—it is straightforward to show that $\lambda^2 = I_4$. The spatial counterpart of the material structural tensor $\boldsymbol{\Lambda}$ is given by $\boldsymbol{\Lambda} = \boldsymbol{n} \otimes \boldsymbol{n}$ while its deviatoric (or volume-preserving) part $\bar{\boldsymbol{\Lambda}}$ is calculated as follows:

$$\bar{\boldsymbol{\Lambda}} = \boldsymbol{\Lambda} - \frac{1}{3}\mathbf{I}. \tag{3}$$

The deviatoric stretch is defined as:

$$\bar{\lambda} = J^{-\frac{1}{3}}\lambda. \tag{4}$$

2.2. Orthogonal decoupled representation of the Cauchy stress tensor

For sake of completeness the essential developments of Lu and Zhang (2005) are exposed here. The concept of splitting the Cauchy stress $\boldsymbol{\sigma}$ into an hydrostatic pressure $\boldsymbol{\sigma}^{\upsilon}$, a deviatoric fibre tension $\boldsymbol{\sigma}^{\bar{\lambda}}$ and a deviatoric tension-free stress in the fibre direction $\hat{\boldsymbol{\sigma}}$ is due to Spencer (1992b):

$$\boldsymbol{\sigma} = \underbrace{\gamma_1 \mathbf{1}}_{\boldsymbol{\sigma}^{\upsilon}} + \underbrace{\gamma_2 \boldsymbol{n}\otimes\boldsymbol{n}}_{\boldsymbol{\sigma}^{\bar{\lambda}}} + \hat{\boldsymbol{\sigma}}. \tag{5}$$

By construction $\hat{\boldsymbol{\sigma}}$ exhibits the following properties:

$$\mathrm{trace}\,(\hat{\boldsymbol{\sigma}}) = 0, \qquad \boldsymbol{n}.\hat{\boldsymbol{\sigma}}\boldsymbol{n} = 0. \tag{6}$$

This is used to calculate the two scalar terms γ_1 and γ_2:

$$\gamma_1 = \frac{\mathrm{trace}(\boldsymbol{\sigma}) - \boldsymbol{\sigma} : \boldsymbol{\Lambda}}{2} \tag{7}$$

$$\gamma_2 = \frac{3\boldsymbol{\sigma} : \boldsymbol{\Lambda} - \mathrm{trace}(\boldsymbol{\sigma})}{2}. \tag{8}$$

This leads to the following definitions:

$$\boldsymbol{\sigma}^{\bar{\lambda}} = \frac{3}{2}(\boldsymbol{\sigma}\bar{\boldsymbol{\Lambda}})\bar{\boldsymbol{\Lambda}} \tag{9}$$

$$\boldsymbol{\sigma}^{\upsilon} = \frac{1}{3}\mathrm{trace}(\boldsymbol{\sigma})I \tag{10}$$

$\hat{\boldsymbol{\sigma}}$ can be written as the sum of two tensors $\hat{\boldsymbol{\sigma}}^1$ and $\hat{\boldsymbol{\sigma}}^2$ defined as follows:

$$\hat{\boldsymbol{\sigma}}^1 = \boldsymbol{n}\hat{\boldsymbol{\sigma}} + \hat{\boldsymbol{\sigma}}\boldsymbol{n} \tag{11}$$

$$\hat{\boldsymbol{\sigma}}^2 = \hat{\boldsymbol{\sigma}} - \hat{\boldsymbol{\sigma}}^1. \tag{12}$$

Injecting Eq. (5) into Eq. (11) leads to:

$$\hat{\boldsymbol{\sigma}}^1 = \boldsymbol{n}\boldsymbol{\sigma} + \boldsymbol{\sigma}\boldsymbol{n} - 2(\boldsymbol{\sigma}\boldsymbol{n})\boldsymbol{n} \tag{13}$$

$$\hat{\boldsymbol{\sigma}}^1\boldsymbol{n} = \boldsymbol{\sigma}\boldsymbol{n} + \boldsymbol{\sigma}(\boldsymbol{n}\otimes\boldsymbol{n})\boldsymbol{n}. \tag{14}$$

Eq. (14) encompasses the fact that $\hat{\boldsymbol{\sigma}}^1$ represents the shear stress in the plane orthogonal to the plane of isotropy – or transverse shear – and can therefore be identified with the fibre-to-fibre and/or matrix-to-fibre shear stress. One can observe that:

$$\hat{\boldsymbol{\sigma}}^2\boldsymbol{n} = \mathbf{0}, \quad \text{and} \tag{15}$$

$$\mathrm{trace}[\hat{\boldsymbol{\sigma}}^2(\mathbf{I} - \boldsymbol{\Lambda})] = 0. \tag{16}$$

Eq. (15) indicates that $\hat{\boldsymbol{\sigma}}^2$ is a plane stress tensor acting in the plane of isotropy in the spatial configuration while Eq. (16) demonstrates that $\hat{\boldsymbol{\sigma}}^2$ is a pure shear tensor (no volumetric contribution or stress along the fibre direction).

The unique decomposition of the Cauchy stress (5) features an important property, notably the fact that the four fictitious symmetric stress tensors $\boldsymbol{\sigma}^{\upsilon}, \boldsymbol{\sigma}^{\bar{\lambda}}, \hat{\boldsymbol{\sigma}}^1$ and $\hat{\boldsymbol{\sigma}}^2$ are mutually orthogonal, i.e.:

$$\begin{aligned} &\boldsymbol{\sigma}^{\upsilon} : \boldsymbol{\sigma}^{\bar{\lambda}} = 0, \qquad \boldsymbol{\sigma}^{\upsilon} : \hat{\boldsymbol{\sigma}}^1 = 0, \qquad \boldsymbol{\sigma}^{\upsilon} : \hat{\boldsymbol{\sigma}}^2 = 0, \\ &\boldsymbol{\sigma}^{\bar{\lambda}} : \hat{\boldsymbol{\sigma}}^1 = 0, \qquad \boldsymbol{\sigma}^{\bar{\lambda}} : \hat{\boldsymbol{\sigma}}^2 = 0, \qquad \hat{\boldsymbol{\sigma}}^1 : \hat{\boldsymbol{\sigma}}^2 = 0. \end{aligned} \tag{17}$$

This means that each of these stress tensors is fully decoupled from the other three and this is a desirable feature if one wants to segregate the volumetric, the deviatoric fibre tensile and the two pure shear stress responses. This can be established by considering the following four fourth-order projection tensors:

$$\mathbb{P}^{\upsilon} = \frac{1}{3}\mathbf{I}\otimes\mathbf{I} \tag{18}$$

$$\mathbb{P}^{\bar{\lambda}} = \frac{3}{2}\bar{\boldsymbol{\Lambda}}\otimes\bar{\boldsymbol{\Lambda}} \tag{19}$$

$$\mathbb{P}^{\hat{\boldsymbol{\sigma}}^1} = \mathbf{I}\boxtimes\boldsymbol{\Lambda} + \boldsymbol{\Lambda}\boxtimes\mathbf{I} - 2\boldsymbol{\Lambda}\otimes\boldsymbol{\Lambda} \tag{20}$$

$$\mathbb{P}^{\hat{\boldsymbol{\sigma}}^2} = \mathbb{I} - \mathbb{P}^{\upsilon} - \mathbb{P}^{\bar{\lambda}} - \mathbb{P}^{\hat{\boldsymbol{\sigma}}^1}. \tag{21}$$

The symbol $\boxtimes$ represents the Kronecker product of second order tensors (Schafer, 1996) defined by:

$$(\mathbf{A}\boxtimes\mathbf{B})_{\alpha\beta} = (\mathbf{A})_{ij}(\mathbf{B})_{kl} \quad \text{where} \begin{cases} \alpha = p(i-1)+k \\ \beta = q(j-1)+l \end{cases}$$
$$\forall A_{m\times n}, B_{p\times q} \text{ second-order tensors.} \tag{22}$$

$\mathbf{A}\boxtimes\mathbf{B}$ is a $mp \times nq$ second-order tensor. See Appendix A for a detailed derivation of $\mathbb{P}^{\hat{\boldsymbol{\sigma}}^1}$. These four projection tensors can be viewed as operators that split the stress space into four distinct subspaces featuring pure volumetric, deviatoric fibre stretch, cross shear and in-plane shear responses.

2.3. Decoupled representation of the deformation gradient

Further to the decoupled representation of the Cauchy stress tensor, the objective is to establish a corresponding kinematic decomposition of the deformation gradient. To this end, $\mathbf{F}$ is written as follows (Lu and Zhang, 2005):

$$\mathbf{F} = J^{\frac{1}{3}}(\delta_1\mathbf{I} + \delta_2\boldsymbol{\Lambda})\hat{\mathbf{F}} \tag{23}$$

where δ_1 and δ_2 are scalars to be determined while $J^{\frac{1}{3}}\delta_1\mathbf{I}, J^{\frac{1}{3}}\delta_2\boldsymbol{\Lambda}, \hat{\mathbf{F}}$ represent respectively the spherical, deviatoric stretching (in the fibre direction) and shear (cross and in-plane) contributions to the deformation gradient. Therefore $\hat{\mathbf{F}}$ must be volume-preserving and stretch-free in the fibre direction:

$$\det(\hat{\mathbf{F}}) = 1 \tag{24}$$

$$\left\|\hat{\mathbf{F}}\boldsymbol{n}_0\right\| = 1. \tag{25}$$

Solving (23) whilst accounting for (24) and (25) leads to:

$$\delta_1 = \frac{1}{\sqrt{\bar{\lambda}}} \tag{26}$$

$$\delta_2 = \bar{\lambda} - \frac{1}{\sqrt{\bar{\lambda}}} = \bar{\lambda} - \delta_1. \tag{27}$$

The decoupled shear deformation gradient is given by:

$$\hat{\mathbf{F}} = \left[\frac{1}{\sqrt{\bar{\lambda}}}(\mathbf{I} - \boldsymbol{\Lambda}) + \frac{1}{\bar{\lambda}}\boldsymbol{\Lambda}\right]J^{-\frac{1}{3}}\mathbf{F}. \tag{28}$$

It is noteworthy that $\hat{\mathbf{F}}$ is expressed using the *spatial* structural tensor $\boldsymbol{\Lambda}$. From (28) one can define the fictitious right and left Cauchy–Green shear deformation tensors:

$$\hat{\mathbf{C}} = \hat{\mathbf{F}}^{\mathrm{T}}\hat{\mathbf{F}} \quad \text{and} \quad \mathbf{b} = \hat{\mathbf{F}}\hat{\mathbf{F}}^{\mathrm{T}}. \tag{29}$$

One can define the principal invariants of $\hat{\mathbf{C}}$:

$$\begin{aligned} &\mathrm{I}_{\hat{\mathbf{C}}} = \mathrm{trace}(\hat{\mathbf{C}}), \qquad \mathrm{II}_{\hat{\mathbf{C}}} = \frac{1}{2}[\mathrm{I}_{\hat{\mathbf{C}}} - \mathrm{trace}(\hat{\mathbf{C}}^2)], \\ &\mathrm{III}_{\hat{\mathbf{C}}} = \det\left(\hat{\mathbf{C}}\right). \end{aligned} \tag{30}$$

The transversely isotropic pseudo-invariants of $\hat{\mathbf{C}}$ are defined as:

$$\mathrm{IV}_{\hat{\mathbf{C}}} = \hat{\mathbf{C}} : \boldsymbol{\Lambda}_0, \qquad \mathrm{V}_{\hat{\mathbf{C}}} = \hat{\mathbf{C}}^2 : \boldsymbol{\Lambda}_0. \tag{31}$$

By construction, $\mathrm{III}_{\hat{\mathbf{C}}} = 1$ and $\mathrm{IV}_{\hat{\mathbf{C}}} = 1$ which implies that only $\mathrm{I}_{\hat{\mathbf{C}}}, \mathrm{II}_{\hat{\mathbf{C}}}$ and $\mathrm{V}_{\hat{\mathbf{C}}}$ can form the *integrity bases* of the transversely isotropic function of $\mathbf{C}$, $\hat{\mathbf{C}}$. It is possible to define a set of

invariants $\left\{\alpha_1(\hat{\mathbf{C}}), \alpha_2(\hat{\mathbf{C}}), \alpha_3(\hat{\mathbf{C}})\right\}$ in one-to-one correspondence with $\left\{\mathrm{I}_{\hat{\mathbf{C}}}, \mathrm{II}_{\hat{\mathbf{C}}}, \mathrm{V}_{\hat{\mathbf{C}}}\right\}$ such that the set $\left\{J, \bar{\lambda}, \alpha_1(\hat{\mathbf{C}}), \alpha_2(\hat{\mathbf{C}}), \alpha_3(\hat{\mathbf{C}})\right\}$ constitutes a set of orthogonal basis functions for $\mathbf{C}$. One such representation is for example (Lu and Zhang, 2005):

$$\alpha_1(\hat{\mathbf{C}}) = \mathrm{trace}\left[\mathrm{III}_{\hat{\mathbf{C}}}\hat{\mathbf{C}}^{-1}(I - \mathbf{\Lambda}_0)\right] \tag{32}$$

$$\alpha_2(\hat{\mathbf{C}}) = \mathrm{V}_{\hat{\mathbf{C}}} \tag{33}$$

$$\alpha_3(\hat{\mathbf{C}}) = \mathrm{II}_{\hat{\mathbf{C}}}. \tag{34}$$

Lu and Zhang (2005) demonstrated that the stress response derived from $\alpha_3(\hat{\mathbf{C}})$ includes both along the fibre and in-plane shear stress which implies a redundant coupling and showed that the stress derived from $\alpha_1(\hat{\mathbf{C}})$ and $\alpha_2(\hat{\mathbf{C}})$ feature respectively an exclusive transverse and along the fibre components. Using Eqs. (28) and (29) one can rewrite $\hat{\mathbf{C}}$ as:

$$\hat{\mathbf{C}} = \frac{J^{\frac{2}{3}}}{\bar{\lambda}}\mathbf{C}^{-1} + \left(1 - \frac{1}{\bar{\lambda}^3}\right)\mathbf{\Lambda}. \tag{35}$$

After some algebraic manipulations $\alpha_1(\hat{\mathbf{C}})$ and $\alpha_2(\hat{\mathbf{C}})$ can be rewritten as:

$$\begin{aligned}\alpha_1 &= \frac{\lambda}{J}\left[\mathrm{trace}(\mathbf{C}) - \frac{1}{\lambda^2}\mathbf{C}^2 : \mathbf{\Lambda}_0\right] \\ &= \sqrt{\frac{I_4}{I_3}}\left(I_1 - \frac{I_5}{I_4}\right) = \frac{I_1 I_4 - I_5}{\sqrt{I_3 I_4}}\end{aligned} \tag{36}$$

$$\alpha_2 = \frac{1}{\lambda^4}\mathbf{C}^2 : \mathbf{\Lambda}_0 = \frac{I_5}{I_4^2} \tag{37}$$

where the previous explicit dependency of these two invariants on $\hat{\mathbf{C}}$ has been replaced by an explicit dependency on the original right Cauchy–Green deformation tensor $\mathbf{C}$ with a slight abuse of notation.

To model the intra-lamellar fibre–fibre interactions of the annulus fibrosus Wagner and Lotz (2004) used the strain energy term $I_5 - I_4^2$. Using kinematic arguments considering the angle between the deformed fibre vector and the vector normal to the deformed differential area element $\mathbf{s}_\perp$ Peng et al. (2006) devised a new invariant characterising the fibre-to-matrix and fibre-to-fibre shear interaction energy.

$$I_\mu = \tan^2\left(\frac{\mathbf{F}\boldsymbol{n}_0}{\|\mathbf{F}\boldsymbol{n}_0\|}, \mathbf{s}_\perp\right) = \frac{I_4}{I_3}\left(I_5 - I_1 I_4 + I_2\right) - 1. \tag{38}$$

However, the model of Peng et al. (2006) was not fully decoupled. The invariant term $I_5 - I_1 I_4 + I_2$ was first established by Schröder and Neff (2003) and was shown to offer the attractive mathematical property of polyconvexity. It was shown that for pure shear deformation I_μ could be reduced to $I_5 - I_4^2$ as in Wagner and Lotz (2004).

A set of four deformation invariants $\mathfrak{S}$ that characterises the fully decoupled response of the kinematic and kinetic tensor quantities has now been established:

$$\begin{aligned}\mathfrak{S} &= \left\{J, \bar{\lambda}, \alpha_1(\mathbf{C}, \mathbf{\Lambda}_0), \alpha_2(\mathbf{C}, \mathbf{\Lambda}_0)\right\} \\ &= \left\{J, \bar{\lambda}, \alpha_1(J, I_1, I_4, I_5), \alpha_2(I_4, I_5)\right\}.\end{aligned} \tag{39}$$

One can postulate the existence of a strain energy function, isotropic function of its scalar-valued tensorial invariants $\mathfrak{S}$ (Boehler, 1978; Spencer, 1992a):

$$\psi = \psi\left[J, \bar{\lambda}, \alpha_1(J, I_1, I_4, I_5), \alpha_2(I_4, I_5)\right]. \tag{40}$$

2.4. Stress tensors

The second Piola–Kirchhoff stress tensor is obtained by differentiation of Eq. (40) with respect to the right Cauchy–Green deformation tensor $\mathbf{C}$:

$$\mathbf{S} = 2\frac{\partial\psi}{\partial\mathbf{C}} = 2\left(\frac{\partial\psi}{\partial J}\frac{\partial J}{\partial\mathbf{C}} + \frac{\partial\psi}{\partial\bar{\lambda}}\frac{\partial\bar{\lambda}}{\partial\mathbf{C}} + \frac{\partial\psi}{\partial\alpha_1}\frac{\partial\alpha_1}{\partial\mathbf{C}} + \frac{\partial\psi}{\partial\alpha_2}\frac{\partial\alpha_2}{\partial\mathbf{C}}\right). \tag{41}$$

If one denotes $\mathfrak{I} = \left\{J, \bar{\lambda}, \alpha_1, \alpha_2\right\}$ as the vector of invariants one can express $\mathbf{S}$ as follows:

$$\mathbf{S} = 2\sum_{i=1}^{4}\frac{\partial\psi}{\partial\mathfrak{I}_i}\mathfrak{B}_i^{\mathbf{S}} \tag{42}$$

where $\mathfrak{B}_i^{\mathbf{S}}$ are the integrity bases of the material symmetry group defined by their set $\mathfrak{B}^{\mathbf{S}}$:

$$\mathfrak{B}^{\mathbf{S}} = \left\{\mathfrak{B}_1^{\mathbf{S}}, \mathfrak{B}_2^{\mathbf{S}}, \mathfrak{B}_3^{\mathbf{S}}, \mathfrak{B}_4^{\mathbf{S}}\right\} = \frac{\partial\mathfrak{I}}{\partial\mathbf{C}}. \tag{43}$$

The Cauchy stress tensor, which is the spatial counterpart of the second Piola–Kirchhoff stress tensor, is calculated from the push-forward operation φ_* (Marsden and Hughes, 1994):

$$\begin{aligned}\boldsymbol{\sigma} &= \frac{1}{J}(\varphi_*\mathbf{S}) = \frac{1}{J}\mathbf{F}\mathbf{S}\mathbf{F}^{\mathrm{T}} = \frac{2}{J}\mathbf{F}\left(\sum_{i=1}^{4}\frac{\partial\psi}{\partial\mathfrak{I}_i}\mathfrak{B}_i^{\mathbf{S}}\right)F^{\mathrm{T}} \\ &= \frac{2}{J}\sum_{i=1}^{4}\frac{\partial\psi}{\partial\mathfrak{I}_i}\mathfrak{B}_i^{\boldsymbol{\sigma}}\end{aligned} \tag{44}$$

where $\mathfrak{B}_i^{\boldsymbol{\sigma}}$ are the integrity bases of the material symmetry group in the spatial configuration:

$$\mathfrak{B}_i^{\boldsymbol{\sigma}} = \varphi_*(\mathfrak{B}_i^{\mathbf{S}}) = \mathbf{F}\left(\mathfrak{B}_i^{\mathbf{S}}\right)\mathbf{F}^{\mathrm{T}}. \tag{45}$$

The integrity bases of $\mathbf{S}$ and $\boldsymbol{\sigma}$ are established in Appendix B.

3. A strain energy function for biological soft tissues

In this section, a novel form of strain energy for biological soft tissues is proposed. First, the function is established for biological materials featuring a transversely isotropic symmetry and later extended to the case of orthotropic symmetry. The motivation behind this formulation is to capture key mechanical characteristics of skin which, across mammalian species, is known to behave like an orthotropic material (Lanir and Fung, 1972). Naturally, the constitutive equations developed are applicable to a wide range of biological and inert materials provided relevant experimental data are available.

Biological soft tissues include a large proportion of collagen which is the main load bearing constituent of the extra-cellular matrix (Fung, 1981). The tropocollagen molecule represents a basic level of the structural hierarchy of collagenous tissues. This long molecule is characterised by a triple helix made of three collagen polypeptide chains wound around one another and strengthened by hydrogen bonds (Buehler, 2008a; Hulmes, 2008). Collagen molecules are further arranged into bundles to form microfibrils which are the building blocks of the next level of the tissue hierarchy: the collagen fibrils.

3.1. Entropic elasticity

A number of authors (Bischoff et al., 2000, 2002a,b; Flynn and McCormack, 2008, 2009; Garikipati et al., 2004, 2006; Kuhl et al., 2005; Kuhl and Holzapfel, 2007) have

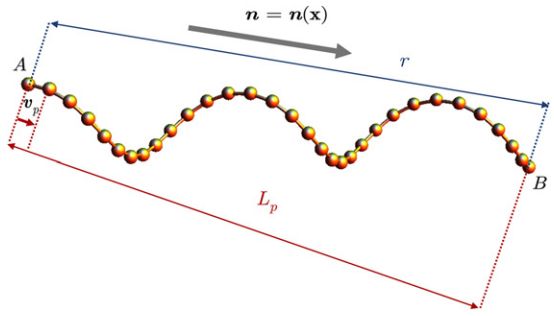

Fig. 1 – Schematic representation of a non-Gaussian entropic chain made of beads connected by rigid links. The chain is characterised by its end-to-end length r, contour length $L = \max(r)$ and persistence length L_p. The persistence length characterises the geometrical smoothness of the chain and can be viewed as the normal projection of the chain along the direction supported by the first link of the chain (vector v_p). AB = rn.

successfully described the mechanics of collagen microfibrils by developing constitutive models based on the so-called worm-like chain model (Kratky and Porod, 1949). The basic idea behind the use of entropic elasticity of macromolecules (Flory, 1969) to represent the mechanical behaviour of collagenous tissues is that collagen molecules aggregated into microfibrils can be viewed as flexible rods that bend smoothly under the influence of thermal fluctuations. Entropy-based constitutive models can account for the anisotropy of biological soft tissues by judicious generalisation of the 8-chain model (Arruda and Boyce, 1993) which was originally developed to model the network behaviour of polymer macromolecules. The 8-chain model is based on a cuboid unit cell containing eight entropic chains linking each corner of the cell to its centre, effectively producing a mechanical network (Kuhl et al., 2005). For this type of approach, shear interactions between collagen fibres are therefore accounted for implicitly in the constitutive formulation. An attractive feature of the worm-like chain model is that, two of its physically meaningful parameters, the persistence and contour length (Fig. 1), are sufficient to produce a great variety of stress response (Kuhl et al., 2005). The free energy of a worm-like chain is:

$$\psi^{\text{entropy}}(r) = \psi_0^{\text{entropy}} + \Re\theta\frac{L}{4L_p}\left(2\frac{r^2}{L^2} + \frac{1}{(1-\frac{r}{L})} - \frac{r}{L}\right) \tag{46}$$

where L, L_p, r_0 and r are respectively the contour, persistence, initial end-to-end length and the current end-to-end length of the chain. $\Re = 1.3806503 \times 10^{-23}$ (m^2 kg s^{-2} K^{-1}) is the Boltzmann constant and θ is the absolute temperature.

ψ_0^{entropy} represents the chain energy in a state of thermodynamic equilibrium. The expression for the entropic energy was obtained by straightforward integration of the entropic force of a single chain with respect to the current end-to-end length r (Kuhl et al., 2005; Kuhl and Holzapfel, 2007; Ogden et al., 2006):

$$\psi^{\text{entropy}}(r) = \int f^{\text{entropy}}(r)\,\mathrm{d}r + \psi_0^{\text{entropy}} \tag{47}$$

$$f^{\text{entropy}}(r) = \frac{\partial\psi^{\text{entropy}}(r)}{\mathrm{d}r} = \Re\theta\frac{1}{4L_p}\left(4\frac{r}{L} + \frac{1}{(1-\frac{r}{L})^2} - 1\right). \tag{48}$$

It must be pointed out that the energy and force of an entropic chain have been normalised by its contour length L as suggested by other researchers (Garikipati et al., 2004; Kuhl et al., 2005; Kuhl and Holzapfel, 2007; Marko and Siggia, 1995; Ogden et al., 2007).

Departing from macroscopic continuum-based modelling approaches for biological soft tissues, Buehler and Wong (2007) studied the mechanics of a single tropocollagen molecule using a combination of atomistic and molecular dynamics simulations. Their model accounted simultaneously for the contributions of entropic elasticity, energetic elasticity and molecular fracture whilst not depending on empirical fitting parameters but rather parameters calculated from first principles physical chemistry. The simulations demonstrated the dominance of elastic entropic effects over energetic effects for the small deformation regime while this trend was reversed at large deformations. The force–stretch curve of a single tropocollagen molecule was in good agreement with optical tweezer-based experiments (Sun et al., 2002, 2004).

3.2. *Decoupled representation of the strain energy function for a transversely isotropic hyperelastic material and hypotheses*

In the present study, it is hypothesised that the mechanics of biological soft tissues featuring transversely isotropy can be described using a continuum composite approach where a family of oriented collagen fibres is embedded into an isotropic matrix. Because of the high water content of biological tissues it is reasonable to assume that the material is nearly incompressible (Fung, 1981). This is a convenient assumption that effectively couples the principal stretches during deformation of the material and therefore simplifies the identification of constitutive parameters.

The novelty of the present approach is that the collagen fibres and the matrix are allowed to interact via *explicit decoupled* shear interactions *whilst* the collagen fibres behave like a worm-like chain model.

Further to the postulate of the existence of a strain energy function $\psi = \psi\left[J, \bar{\lambda}, \alpha_1(J, I_1, I_4, I_5), \alpha_2(I_4, I_5)\right]$ (Eq. (40)), it is assumed that the strain energy function takes an additive representation:

$$\begin{aligned}\psi &= f(J, \bar{\lambda}, \alpha_1(\mathbf{C}), \alpha_2(\mathbf{C})) \\ &= \psi^{\upsilon}(J) + \psi^{\bar{\lambda}}(\bar{\lambda}) + \hat{\psi}\left[\alpha_1(\mathbf{C}), \alpha_2(\mathbf{C})\right].\end{aligned} \tag{49}$$

A worm-like chain model is used to describe the mechanical behaviour of collagen assemblies/fibres. Collagen fibres are assumed to deform incompressibly and, when this assumption is combined with a principle of affinity for the chains, one can relate the (macroscopic) deviatoric stretch $\bar{\lambda}$ to the (nanoscopic) measure of the end-to-end chain length in the reference and current configurations:

$$\bar{\lambda} = \frac{r}{r_0}. \tag{50}$$

This leads to restrictions on the possible values of $\bar{\lambda}$:

$$0 < r < L \Rightarrow 0 < \bar{\lambda} < \frac{L}{r_0}. \tag{51}$$

The end-to-end length of the chain cannot exceed its contour length. One can define extension ratios $z = r/L$ and $z_0 = r_0/L$

(Ogden et al., 2006). Substituting (50) into (46) and (48) leads to an entropic energy function of the macroscopic deviatoric stretch:

$$\psi^{\bar{\lambda}}_{\text{chain}}(\bar{\lambda}) = \aleph\theta\frac{L}{4L_p}\left(2\frac{\bar{\lambda}^2 r_0^2}{L^2} + \frac{1}{\left(1-\frac{\bar{\lambda}r_0}{L}\right)} - \frac{\bar{\lambda}r_0}{L}\right) + \psi_0^{\text{entropy}} \quad (52)$$

$$f^{\bar{\lambda}}_{\text{chain}}(\bar{\lambda}) = \aleph\theta\frac{1}{4L_p}\left(4\frac{\bar{\lambda}r_0}{L} + \frac{1}{\left(1-\frac{\bar{\lambda}r_0}{L}\right)^2} - 1\right). \quad (53)$$

A repulsion energy is introduced to prevents the chain to collapse onto itself and to ensure the existence of a natural reference state where the total strain energy and the stress vanish.

$$\psi^{\bar{\lambda}}_{\text{repulsion}}(\bar{\lambda}) = \xi_0 \ln(\bar{\lambda}^{r_0^2}). \quad (54)$$

If $\aleph$ is the chain density per unit volume, the total chain energy per unit volume is:

$$\begin{aligned}\psi^{\bar{\lambda}}(\bar{\lambda}) &= \aleph\left[\psi^{\bar{\lambda}}_{\text{chain}}(\bar{\lambda}) + \psi^{\bar{\lambda}}_{\text{repulsion}}(\bar{\lambda})\right] \\ &= \aleph\aleph\theta\frac{L}{4L_p}\left(2\frac{\bar{\lambda}^2 r_0^2}{L^2} + \frac{1}{\left(1-\frac{\bar{\lambda}r_0}{L}\right)} - \frac{\bar{\lambda}r_0}{L}\right) \\ &\quad + \xi_0\aleph\ln(\bar{\lambda}^{r_0^2})\end{aligned} \quad (55)$$

$$\text{where } \xi_0 = -\frac{\aleph\theta L}{4L_p}\frac{r_0^2(6L^2r_0^2 - 9Lr_0^4 + 4r_0^6)}{L^2(L-r_0^2)^2} \quad (56)$$

$$\xi_0 = -\frac{\aleph\theta L}{4L_p}\frac{z_0^2(6 - 9z_0 + 4z_0^2)}{z_0^2(z_0-1)^2}. \quad (57)$$

It is generally assumed that due to their rod-like shape factor, collagen fibres buckle under infinitesimal compressive stretch and are therefore unable to sustain compressible load along their principal axis. For this reason, fibre energy functions are often defined as piece-wise functions vanishing under compressive stretch ($\lambda < 1$) (Blemker et al., 2005; Holzapfel et al., 2000; Limbert et al., 2003, 2004; Peng et al., 2006; Wagner and Lotz, 2004; Weiss et al., 1996). Some authors have challenged this approach by introducing explicitly the stiffness of collagen fibres into their constitutive formulation (Guo et al., 2006; Tang et al., 2009). Here a similar line of thought is followed by considering collagen fibres under compression as incompressible neo-Hookean solids with a shear modulus μ_0:

$$\psi^{\bar{\lambda}}(\bar{\lambda}) = \begin{cases} \aleph\mu_0\left(\bar{\lambda}^2 + \frac{2}{\bar{\lambda}} - 3\right) + \xi_0\aleph\ln(\bar{\lambda}^{r_0^2}) & \text{if } \bar{\lambda} \le 1 \\ \aleph\aleph\theta\frac{L}{4L_p}\left(2\frac{\bar{\lambda}^2 r_0^2}{L^2} + \frac{1}{\left(1-\frac{\bar{\lambda}r_0}{L}\right)} - \frac{\bar{\lambda}r_0}{L}\right) & \\ \quad + \xi_0\aleph\ln(\bar{\lambda}^{r_0^2}) \quad \text{if } \bar{\lambda} > 1. & \end{cases} \quad (58)$$

The volumetric energy is defined by the following function (Ogden, 1972; Simo and Miehe, 1992):

$$\psi^{\upsilon}(J) = \frac{1}{4}\kappa(J^2 - 2\ln J - 1) \quad (59)$$

where κ is the bulk modulus of the matrix.

It is further assumed that the shear energy takes an additive decomposition into the sum of isotropic shear energy in the plane of material isotropy $\hat{\psi}^1$ (transverse to the fibre direction) and anisotropic shear energy $\hat{\psi}^2$:

$$\hat{\psi}\left[\alpha_1(\mathbf{C}), \alpha_2(\mathbf{C})\right] = \hat{\psi}^1(\alpha_1(\mathbf{C})) + \hat{\psi}^2(\alpha_2(\mathbf{C})). \quad (60)$$

The anisotropic shear energy encompasses the matrix-to-fibre and fibre-to-fibre shear interactions.

The isotropic shear energy is defined as follows:

$$\hat{\psi}^1(\alpha_1) = \frac{1}{2}\mu_1(\alpha_1 - 2). \quad (61)$$

The anisotropic shear energy is defined as follows:

$$\hat{\psi}^2(\alpha_2) = \frac{1}{2}\mu_2(\alpha_2 - 1)^2. \quad (62)$$

This latter form of shear energy implies that there is no coupling between the amount of stretch along the fibres and the fibre-to-fibre/matrix-to-fibre shear energy. Peng et al. (2006) used a scaling sigmoid term depending on the fibre stretch to weight the shear interaction strain energy. This was motivated by the fact that, under low stretch or compression, collagen fibres offer little resistance to bending and rotation while this trend is reversed at large stretch when fibres stiffen and the influence of cross-links becomes significant (Fujita et al., 2000). $\hat{\psi}^2(\alpha_2)$ is therefore modified and re-written as:

$$\tilde{\psi}(\alpha_2, \bar{\lambda}) = f_\mu(\bar{\lambda}) \times \hat{\psi}^2(\alpha_2) = \frac{1}{2}\mu_2(\alpha_2 - 1)^2 f_\mu(\bar{\lambda}) \quad (63)$$

where $f_\mu(\bar{\lambda})$ is a normalised sigmoid function with constitutive parameters a, b and $\bar{\lambda}_c$:

$$f_\mu(\bar{\lambda}) = \frac{1}{1 + a\,e^{-b(\bar{\lambda}-\bar{\lambda}_c)}} \quad (64)$$

$\bar{\lambda}_c$ is a critical deviatoric stretch at which cross-links between micro-fibrils get recruited while a and b control the shape of the sigmoid function.

The total energy of the composite material is then defined:

$$\psi(J, \bar{\lambda}, \alpha_1, \alpha_2) = \psi^{\bar{\lambda}}(\bar{\lambda}) + \psi^{\upsilon}(J) + \hat{\psi}^1(\alpha_1) + \tilde{\psi}(\alpha_2, \bar{\lambda}). \quad (65)$$

The derivatives of $\psi(J, \bar{\lambda}, \alpha_1, \alpha_2)$ with respect to each of its arguments are required to calculate material and spatial stress tensors:

$$\frac{\partial\psi^{\bar{\lambda}}(\bar{\lambda})}{\partial\bar{\lambda}} = \begin{cases} \aleph\mu_0\left(2\bar{\lambda} - \frac{2}{\bar{\lambda}^2}\right) & \text{if } \bar{\lambda} \le 1 \\ \aleph\aleph\theta\frac{L}{4L_p}\left(4\frac{\bar{\lambda}r_0^2}{L^2} + \frac{1}{\left(1-\frac{\bar{\lambda}r_0}{L}\right)^2} - \frac{r_0}{L}\right) & \\ \quad + \xi_0\aleph\ln(\bar{\lambda}^{r_0^2}) \quad \text{if } \bar{\lambda} > 1 & \end{cases} \quad (66)$$

$$\frac{\partial\psi^{\upsilon}(J)}{\partial J} = \frac{1}{2}\kappa\frac{J^2 - 1}{J} \quad (67)$$

$$\frac{\partial\hat{\psi}^1(\alpha_1)}{\partial\alpha_1} = \frac{1}{2}\mu_1 \quad (68)$$

$$\frac{\partial\tilde{\psi}(\alpha_2, \bar{\lambda})}{\partial\alpha_2} = \mu_2(\alpha_2 - 1)f_\mu(\bar{\lambda}) \quad (69)$$

$$\frac{\partial\tilde{\psi}(\alpha_2, \bar{\lambda})}{\partial\bar{\lambda}} = \frac{1}{2}\mu_2(\alpha_2 - 1)^2\frac{ab\,e^{-b(\bar{\lambda}-\bar{\lambda}_c)}}{\left(1 + a\,e^{-b(\bar{\lambda}-\bar{\lambda}_c)}\right)^2}. \quad (70)$$

The second Piola–Kirchhoff and Cauchy stress tensors can be written as:

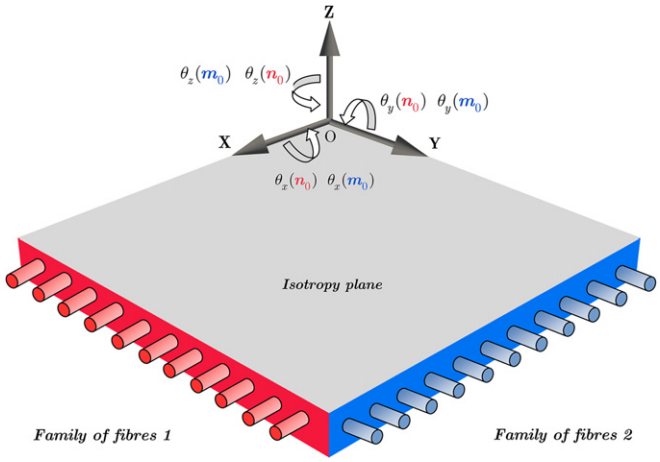

Fig. 2 – Schematic representation of a continuum orthotropic composite made of two families of fibre embedded into an isotropic matrix. In the reference configuration, the two unit vectors n_0 and m_0 are orthogonal to each other and orthogonal to the vector Z. The sketch also represents the skin tissue sample used in the finite element analyses (Section 5). The faces indicated in red and blue correspond respectively to the directions orthogonal to the head-to-tail direction (family of fibres 1) and the direction orthogonal to it (family of fibres 2). (For interpretation of the references to colour in this figure legend, the reader is referred to the web version of this article.)

$$\mathbf{S} = 2\left[\frac{\partial\psi^{\upsilon}(J)}{\partial J}\mathfrak{B}_1^{\mathbf{S}} + \left(\frac{\partial\psi^{\bar{\lambda}}(\bar{\lambda})}{\partial\bar{\lambda}} + \frac{\partial\tilde{\psi}(\alpha_2,\bar{\lambda})}{\partial\bar{\lambda}}\right)\mathfrak{B}_2^{\mathbf{S}} + \frac{\partial\hat{\psi}^1(\alpha_1)}{\partial\alpha_1}\mathfrak{B}_3^{\mathbf{S}} + \frac{\partial\tilde{\psi}(\alpha_2,\bar{\lambda})}{\partial\alpha_2}\mathfrak{B}_4^{\mathbf{S}}\right] \tag{71}$$

$$\boldsymbol{\sigma} = \frac{2}{J}\left[\frac{\partial\psi^{\upsilon}(J)}{\partial J}\mathfrak{B}_1^{\sigma} + \left(\frac{\partial\psi^{\bar{\lambda}}(\bar{\lambda})}{\partial\bar{\lambda}} + \frac{\partial\tilde{\psi}(\alpha_2,\bar{\lambda})}{\partial\bar{\lambda}}\right)\mathfrak{B}_2^{\sigma} + \frac{\partial\hat{\psi}^1(\alpha_1)}{\partial\alpha_1}\mathfrak{B}_3^{\sigma} + \frac{\partial\tilde{\psi}(\alpha_2,\bar{\lambda})}{\partial\alpha_2}\mathfrak{B}_4^{\sigma}\right]. \tag{72}$$

3.3. Decoupled representation of the strain energy function for an orthotropic hyperelastic material and hypotheses

It is now assumed that soft tissues can be represented as a continuum composite material featuring two families of oriented collagen fibres embedded in a compliant matrix of proteoglycans. These two families of fibres are defined by their local unit vector $\boldsymbol{n}_0 = \boldsymbol{n}_0(\mathbf{X})$ and $\boldsymbol{m}_0 = \boldsymbol{m}_0(\mathbf{X})$ in the reference configuration (Fig. 2). One can then define their corresponding structural tensors $\boldsymbol{\Lambda}^{\boldsymbol{n}_0} = \boldsymbol{n}_0 \otimes \boldsymbol{n}_0$ and $\boldsymbol{\Lambda}^{\boldsymbol{m}_0} = \boldsymbol{m}_0 \otimes \boldsymbol{m}_0$. In order to lighten up the equations the convention that the Greek letter β stands for either $\boldsymbol{n}_0$ or $\boldsymbol{m}_0$ is adopted. The subscript and superscript β are therefore used to distinguish each family of fibres and their associated quantities: invariants, energy functions and constitutive parameters. Following Eq. (2) one can define the anisotropic invariants $\left\{I_4^{\beta}\right\}_{\beta=1,2}$ and $\left\{I_5^{\beta}\right\}_{\beta=1,2}$:

$$I_4^{\beta} = \mathbf{C} : \boldsymbol{\Lambda}^{\beta} = \lambda_{\beta}^2 = J^{\frac{2}{3}}\bar{\lambda}_{\beta}^2, \qquad I_5^{\beta} = \mathbf{C}^2 : \boldsymbol{\Lambda}^{\beta}. \tag{73}$$

Following Eqs. (36) and (37) four shear invariants are defined:

$$\alpha_1^{\beta} = \frac{I_1 I_4^{\beta} - I_5^{\beta}}{\sqrt{I_3 I_4^{\beta}}}, \qquad \alpha_2^{\beta} = \frac{1}{\lambda_{\beta}^4}\mathbf{C}^2 : \boldsymbol{\Lambda}^{\beta} = \frac{I_5^{\beta}}{(I_4^{\beta})^2}. \tag{74}$$

The total strain energy of the composite material is then expressed as:

$$\psi = \psi^{\upsilon}(J) + \sum_{\beta=1}^{2}\left[\psi^{\bar{\lambda}}_{\beta}(\bar{\lambda}_{\beta}) + \hat{\psi}^1_{\beta}(\alpha_1^{\beta}) + \tilde{\psi}^2_{\beta}(\alpha_2^{\beta},\bar{\lambda}_{\beta})\right] \tag{75}$$

where $r_{0\beta}$ is the initial end-to-end length of the entropic chain relative to the family of fibre β and:

$$f_{\mu}^{\beta}(\bar{\lambda}_{\beta}) = \frac{1}{1 + a_{\beta}\,\mathrm{e}^{-b_{\beta}(\bar{\lambda}_{\beta} - \bar{\lambda}_{\beta}^{\mathrm{c}})}} \tag{76}$$

$$\hat{\psi}^1_{\beta}(\alpha_1^{\beta}) = \frac{1}{2}\mu_1^{\beta}\left(\alpha_1^{\beta} - 2\right) \tag{77}$$

$$\tilde{\psi}^2_{\beta}(\alpha_2^{\beta},\bar{\lambda}_{\beta}) = f_{\mu}^{\beta}(\bar{\lambda}) \times \hat{\psi}^2(\alpha_2) = \frac{1}{2}\mu_2^{\beta}\left(\alpha_2^{\beta} - 1\right)^2 f_{\mu}^{\beta}(\bar{\lambda}_{\beta}) \tag{78}$$

$$\xi_0^{\beta} = -\frac{\aleph\theta L_{\beta}}{4L_p}\frac{r_{0\beta}^2(6L_{\beta}^2 r_{0\beta}^2 - 9L_{\beta}r_{0\beta}^4 + 4r_{0\beta}^6)}{L_{\beta}^2(L_{\beta} - r_{0\beta}^2)^2} \tag{79}$$

$$\psi^{\bar{\lambda}}_{\beta}(\bar{\lambda}_{\beta}) = \begin{cases} \aleph_{\beta}\mu_0^{\beta}\left(\bar{\lambda}_{\beta}^2 + \dfrac{2}{\bar{\lambda}_{\beta}} - 3\right) + \xi_0^{\beta}\aleph_{\beta}\ln(\bar{\lambda}^{r_{0\beta}^2}) & \text{if } \bar{\lambda}_{\beta} \le 1 \\ \aleph_{\beta}\aleph\theta\dfrac{L_{\beta}}{4L_p^{\beta}}\left(2\dfrac{\bar{\lambda}_{\beta}^2 r_{0\beta}^2}{L_{\beta}^2} + \dfrac{1}{\left(1 - \frac{\bar{\lambda}_{\beta}r_{0\beta}}{L_{\beta}}\right)} - \dfrac{\bar{\lambda}_{\beta}r_{0\beta}}{L_{\beta}}\right) & \\ \quad + \xi_0^{\beta}\aleph_{\beta}\ln(\bar{\lambda}_{\beta}^{r_{0\beta}^2}) \quad \text{if } \bar{\lambda}_{\beta} > 1. \end{cases} \tag{80}$$

The orthotropic constitutive model results in a set of 23 constitutive parameters:

$$\mathbf{p} = \{\aleph, \theta, \kappa, \mu_0^{\beta}, \mu_1^{\beta}, \mu_2^{\beta}, \aleph_{\beta}, L_{\beta}, L_p^{\beta}, r_{\beta}, a_{\beta}, b_{\beta}, \bar{\lambda}_{\beta}^{\mathrm{c}}\}_{\beta=1,2}. \tag{81}$$

In the next section, further assumptions will be made to reduce the number of material parameters.

The second Piola–Kirchhoff and Cauchy stress tensors can be written as:

Table 1 – Material parameters for the constitutive model (subset p^1).

Boltzmann constant	$\mathfrak{K}$	1.3806503×10^{-23} ($\mathrm{m^2\,kg\,s^{-2}\,K^{-1}}$)
Absolute temperature	θ	310 (K)
Bulk modulus of the matrix	κ	50 (kPa)
Compressive stiffness of collagen fibres	μ_0	0 (Pa)
Shape parameter for sigmoid coupling function 1 and 2	a	50
Shape parameter for sigmoid coupling function 1 and 2	b	20
Density of chains (Fibre family 1)	$\aleph_{n_0}$	$7\cdot10^{21}$ ($\mathrm{m^{-3}}$)
Density of chains (Fibre family 2)	$\aleph_{m_0}$	$7\cdot10^{21}$ ($\mathrm{m^{-3}}$)
Shape parameter for sigmoid coupling function 1	$\bar{\lambda}^{\mathrm{c}}_{n_0}$	1.15
Shape parameter for sigmoid coupling function 1	$\bar{\lambda}^{\mathrm{c}}_{m_0}$	1.40

$$\mathbf{S} = 2\frac{\partial\psi^{v}(J)}{\partial J}\mathfrak{B}^{\mathbf{S}}_1 + 2\sum_{\beta=1}^{2}\left[\left(\frac{\partial\psi^{\bar{\lambda}}(\bar{\lambda}_\beta)}{\partial\bar{\lambda}_\beta}+\frac{\partial\tilde{\psi}(\alpha^\beta_2,\bar{\lambda}_\beta)}{\partial\bar{\lambda}_\beta}\right)\mathfrak{B}^{\mathbf{S}^\beta}_2 + \frac{\partial\hat{\psi}^1_\beta(\alpha^\beta_1)}{\partial\alpha^\beta_1}\mathfrak{B}^{\mathbf{S}^\beta}_3 + \frac{\partial\tilde{\psi}^2_\beta(\alpha^\beta_2,\bar{\lambda}_\beta)}{\partial\alpha^\beta_2}\mathfrak{B}^{\mathbf{S}^\beta}_4\right] \tag{82}$$

$$\boldsymbol{\sigma} = \frac{2}{J}\frac{\partial\psi^{v}(J)}{\partial J}\mathfrak{B}^{\boldsymbol{\sigma}}_1 + \frac{2}{J}\sum_{\beta=1}^{2}\left[\left(\frac{\partial\psi^{\bar{\lambda}}(\bar{\lambda}_\beta)}{\partial\bar{\lambda}_\beta}+\frac{\partial\tilde{\psi}(\alpha^\beta_2,\bar{\lambda}_\beta)}{\partial\bar{\lambda}_\beta}\right)\mathfrak{B}^{\boldsymbol{\sigma}^\beta}_2 + \frac{\partial\hat{\psi}^1_\beta(\alpha^\beta_1)}{\partial\alpha^\beta_1}\mathfrak{B}^{\boldsymbol{\sigma}^\beta}_3 + \frac{\partial\tilde{\psi}^2_\beta(\alpha^\beta_2,\bar{\lambda}_\beta)}{\partial\alpha^\beta_2}\mathfrak{B}^{\boldsymbol{\sigma}^\beta}_4\right]. \tag{83}$$

The first Piola–Kirchhoff stress tensor – also called nominal stress tensor – is obtained by transformation of the second Piola–Kirchhoff stress tensor according to $\mathbf{P}=\mathbf{FS}$ (Holzapfel, 2000):

$$\mathbf{P} = 2\frac{\partial\psi^{v}(J)}{\partial J}\mathbf{F}\mathfrak{B}^{\mathbf{S}}_1 + 2\sum_{\beta=1}^{2}\left[\left(\frac{\partial\psi^{\bar{\lambda}}(\bar{\lambda}_\beta)}{\partial\bar{\lambda}_\beta}+\frac{\partial\tilde{\psi}(\alpha^\beta_2,\bar{\lambda}_\beta)}{\partial\bar{\lambda}_\beta}\right)\mathbf{F}\mathfrak{B}^{\mathbf{S}^\beta}_2 + \frac{\partial\hat{\psi}^1_\beta(\alpha^\beta_1)}{\partial\alpha^\beta_1}\mathbf{F}\mathfrak{B}^{\mathbf{S}^\beta}_3 + \frac{\partial\tilde{\psi}^2_\beta(\alpha^\beta_2,\bar{\lambda}_\beta)}{\partial\alpha^\beta_2}\mathbf{F}\mathfrak{B}^{\mathbf{S}^\beta}_4\right]. \tag{84}$$

The nominal traction vectors along the fibre directions $\boldsymbol{n}_0$ and $\boldsymbol{m}_0$ are defined as:

$$\mathbf{P}^{\parallel} = \mathbf{P}\boldsymbol{n}_0 \tag{85}$$

$$\mathbf{P}^{\perp} = \mathbf{P}\boldsymbol{m}_0. \tag{86}$$

4. Identification of constitutive parameters

Data from experimental uniaxial tensile tests performed on rabbit skin (Lanir and Fung, 1972) were used to identify a set of constitutive parameters for the prototype material law described in the Section 3.3. Data consisted of uniaxial tensions along the head-to-tail direction ($\bar{\lambda}_{\mathrm{i}}, \bar{\mathrm{y}}^{\parallel}_{\mathrm{i}}$) (superscript $\parallel$) and perpendicular to it ($\bar{\lambda}_{\mathrm{i}}, \bar{\mathrm{y}}^{\perp}_{\mathrm{i}}$) (superscript $\perp$).

$$\mathfrak{O}(\mathbf{p}) = \sum_{\mathrm{i}=1}^{n}\left(\mathrm{P}^{\parallel}(\bar{\lambda}_{\mathrm{i}}) - \bar{\mathrm{y}}^{\parallel}_{\mathrm{i}}\right)^2 + \sum_{\mathrm{j}=1}^{m}\left(\mathrm{P}^{\perp}(\bar{\lambda}_{\mathrm{j}}) - \bar{\mathrm{y}}^{\perp}_{\mathrm{j}}\right)^2. \tag{87}$$

The identification process consists in finding the set of constitutive parameters that minimise the function $\mathfrak{O}(\mathbf{p})$. The optimisation was performed using a constrained non-linear optimisation procedure using a global hill-climbing algorithm (Global Optimization 8, Loehle Enterprises, Naperville, IL, USA) within the MATHEMATICA ® 7 environment (Wolfram Research Inc., Champaign, IL, USA).

The initial vector $\mathbf{p}$ (Eq. (81)) containing all the constitutive parameters was further split into two subsets $\mathbf{p}^1 = \left\{\mathfrak{K}, \theta, \kappa, \mu_0, a, b, \aleph_{n_0}, \aleph_{m_0}, \bar{\lambda}^{\mathrm{c}}_{n_0}, \bar{\lambda}^{\mathrm{c}}_{m_0}\right\}$ and $\mathbf{p}^2 = \{\mu_1, \mu_2, L_{n_0}, L^{n_0}_p, r_{n_0}, \aleph_{m_0}, L_{m_0}, L^{m_0}_p, r_{m_0}\}$. This was based on the following assumptions:

$$\mu_0 = \mu_0^{n_0} = \mu_0^{m_0} = 0 \tag{88}$$

$$\mu_1 = \mu_1^{n_0} = \mu_1^{m_0}, \qquad \mu_2 = \mu_2^{n_0} = \mu_2^{m_0} \tag{89}$$

$$a = a_1 = a_2 = 50, \qquad b = b_1 = b_2 = 20 \tag{90}$$

$$\aleph_{n_0} = \aleph_{m_0} = 7\cdot10^{21} \tag{91}$$

$$\bar{\lambda}^{\mathrm{c}}_{n_0} = 1.4, \qquad \bar{\lambda}^{\mathrm{c}}_{m_0} = 1.8. \tag{92}$$

Herein, it was assumed that the axial compressive stiffness of collagen fibres was negligible (Eq. (88)) whilst both families of fibres had the same shear properties (Eqs. (89) and (90)) and fibre density (as chosen in Kuhl et al. (2005), equation). The vector $\mathbf{p}^1$ was fixed from the outset (Eqs. (90) and (92)) (Table 1) while $\mathbf{p}^2$ was determined via an optimisation procedure. Results of the identification procedure are presented on Fig. 4 by overlaying the theoretical nominal stress in the fibre directions over the experimental stress. Once the identification process is completed, the goodness of fit between the theoretical and experimental stress is assessed using the correlation coefficient ρ.

5. Finite element analyses

The orthotropic constitutive model described in Section 3 was implemented in a 64bit-based non-linear finite element framework within MATHEMATICA ® by developing a customised linear 8-noded hexahedral element using an enhanced strain formulation which has been proven to be superior to a standard displacement-based formulation, particularly for shear-dominated problems and nearly incompressible materials (Korelc et al., 2010). A series of finite element analyses was conducted to assess some aspects of the mechanical response of the constitutive model developed in Section 3. Particular emphasis was placed on the shear stress responses for various loading scenarios.

5.1. *Influence of the fibre direction*

In fibrous biological soft tissues, the directions of anisotropy arising from oriented fibres are key in governing the mechanical response. To assess the effect of the orientation of the fibre families 1 and 2 on the response of respectively σ_{xx} and σ_{yy} during a homogeneous extension along these directions, a simple parametric analysis was conducted by varying each initial fibre orientation from 0 to $\pi/2$ rad.

Table 2 – Material parameters for the constitutive model (subset p^2). The contour, persistence and initial lengths were normalised and are therefore dimensionless (see Section 3.1).

Matrix shear modulus	μ_1	150.123 (Pa)
Maximum fibre–fibre/matrix–fibre shear modulus	μ_2	9.981 (Pa)
Contour length of a tropocollagen molecule	L_{n_0}	2.792
Persistence length of a tropocollagen molecule	$L_p^{n_0}$	0.200
Initial length of a crimpled collagen molecule	r_{0n_0}	1.368
Contour length of a tropocollagen molecule	$L_{m_0} = L_{n_0}$	2.792
Persistence length of a tropocollagen molecule	$L_p^{m_0}$	0.591
Initial length of a crimpled collagen molecule	r_{0m_0}	1.741

Table 3 – Characteristics of shear modes (see Fig. 2).

Shear mode	Shear plane	Shear direction
1	(OX, OY)	**X**
2	(OX, OY)	**Y**
3	(OX, OZ)	**Y**
4	(OX, OZ)	**Z**
5	(OY, OZ)	**X**
6	(OY, OZ)	**Z**

5.2. *Simple shear stress response for the 6 shear modes*

A parallelepiped geometry acting as a surrogate for a skin tissue sample (dimensions: 10 × 10 × 1 (mm^3), see Fig. 2) was generated and meshed with 50,000 8-noded hexahedral elements. Six simple shear modes were considered (Table 3) and simulated for a maximum shear strain of 0.5. The fibre directions were aligned with the principal directions *X* and *Y* (see indications on Fig. 2).

5.3. *Sensitivities of the shear response for an indentation test*

The finite element mesh described in the previous section was also used to simulate an indentation test. This type of loading scenario provides a very useful insight into the mechanical response of orthotropic materials because it solicits the biaxial fibre and multi-plane/multi-direction shear responses. The test was simulated by applying a 0.2 mm vertical displacement on a small patch located at the centre of the top surface of the sample (dimension of the patch: 0.5 × 0.5 (mm^2)). The planes parallel to this surface corresponds to the isotropy plane of the material. Moreover, indentation testing is widely used to characterise the mechanical properties of biological tissues, particularly those of skin (Delalleau et al., 2006).

For the indentation analysis a direct numerical sensitivity analysis was performed. In a finite element context, the object of a sensitivity analysis is to calculate the dependence of a functional response $\mathfrak{R}(\mathbf{q}) = \{\Re_1(\mathbf{q}), \Re_2(\mathbf{q}), \ldots, \Re_s(\mathbf{q})\}$ made of *s* scalars on *n* parameters $\mathbf{q} = \{q_1, q_2, \ldots, q_n\}$ which are generally arbitrary analysis model inputs but can also be arbitrary intermediate or final results of the analysis. This is achieved by calculating the local partial derivatives of the functional response with respect to the parameters leading to a sensitivity matrix $\mathfrak{S}$:

$$\mathfrak{S} = \frac{\partial \mathfrak{R}(\mathbf{q})}{\partial \mathbf{q}}. \tag{93}$$

The physical interpretation of a calculated sensitivity is that it provides the quantitative change of the response variable as result of a unit change in the parameter considered. In the context of this study a numerical subroutine was developed to calculate the sensitivities of the Cauchy shear stress components (σ_{xy}, σ_{xz} and σ_{yz}) with respect to the 18 parameters of the constitutive model (Eq. (94)) and the 3 orientation angles of each fibre direction unit vector (Eq. (95)) (the angles are defined on Fig. 2):

$$\begin{aligned}\mathbf{p} = \{&\Re, \theta, \kappa, \mu_0, a, b, \bar{\lambda}^c_{n_0}, \bar{\lambda}^c_{m_0}, \mu_1, \mu_2, \aleph_{n_0},\\ &L_{n_0}, L_p^{n_0}, r_{n_0}, \aleph_{m_0}, L_{m_0}, L_p^{m_0}, r_{m_0}\}\end{aligned} \tag{94}$$

$$\mathbf{p}^3 = (\theta_x^{n_0}, \theta_y^{n_0}, \theta_z^{n_0}, \theta_x^{m_0}, \theta_y^{m_0}, \theta_z^{m_0}). \tag{95}$$

The vector of parameters $\check{\mathbf{p}}$ is defined as follows: $\check{\mathbf{p}} = \mathbf{p} \cup \mathbf{p}^3$. For the sensitivity analysis considered in this study the response vector is made of the three shear stress components of the Cauchy stress tensor $\boldsymbol{\sigma}$:

$$\mathfrak{R}(\check{\mathbf{p}}) = \left\{\sigma_{xy}(\check{\mathbf{p}}), \sigma_{xz}(\check{\mathbf{p}}), \sigma_{yz}(\check{\mathbf{p}})\right\}. \tag{96}$$

The sensitivity matrix $\mathfrak{S} = \partial \mathfrak{R}(\check{\mathbf{p}})/\partial \check{\mathbf{p}}$ is calculated at each integration point of each element and, consequently, a sensitivity analysis require a large number of additional computations. For example, for the mesh considered in the present finite element analyses, 8 million sensitivity values are calculated for each of the three scalar response variables (3 shear stress components). The current finite element implementation offers the added advantage that the sensitivity values can be mapped onto the geometry/mesh and represented using standard colour contouring visualisation techniques.

6. Results and discussion

6.1. *Parameter identification*

The prescribed and identified constitutive parameters are listed respectively in Tables 1 and 2. These sets of parameters leads to a good agreement between the theoretical and experimental stress curves as highlighted on Fig. 4. The correlation coefficient was 0.998 and 0.997 for the stress respectively along the head-to-tail fibre direction and the direction perpendicular to it. The constitutive formulation proposed is capable of capturing well the orthotropic behaviour of skin due to the presence of two distinct families of collagen fibres. The characteristics locking stretch of each family of collagen fibres is captured nicely. The fibre-to-fibre and matrix-to-fibre shear interactions are accounted for via

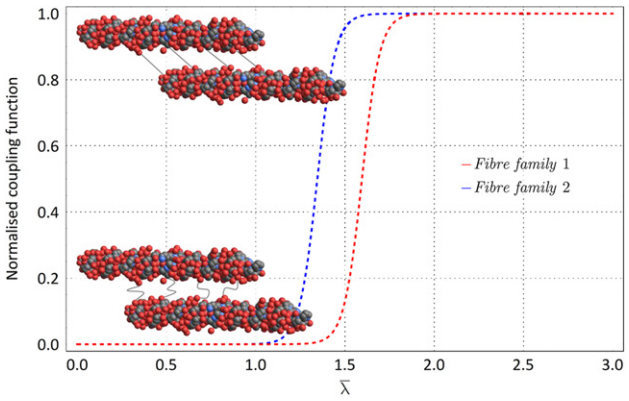

Fig. 3 – Normalised sigmoid function characterising the stiffening of the fibre-to-fibre shear modulus. Conceptualisation of the shear interactions occurring between two tropocollagen molecules. The molecular representation for tropocollagen is obtained from the Protein Data Bank file `1QSU.pdb` (www.pdb.org): crystal structure of the triple-helical collagen-like peptide C, (PRO-HYP-GLY)4-GLU-LYS-GLY(PRO-HYP-GLY)5 (Kramer et al., 2000).

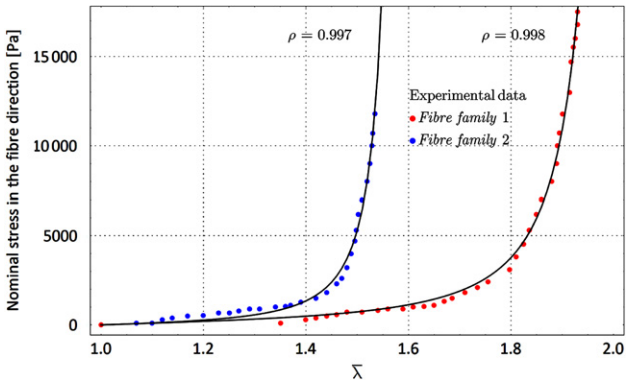

Fig. 4 – Experimental data from uniaxial tensile tests on rabbit skin from Lanir and Fung (1972) and the corresponding theoretical values (continuous lines) calculated after identification of the constitutive parameters.

a dedicated invariant $\alpha_2(\hat{\mathbf{C}})$ (Eq. (37)) which is further used to couple these shear interactions with extension along the deviatoric stretches in each fibre direction via the sigmoid normalised function $f_\mu^\beta(\bar{\lambda}_\beta)$. The locking characteristics of the sigmoid function are directly linked to the specific locking stretch associated with each fibre family (Fig. 3).

Fibre density ($\aleph_{n_0} = \aleph_{m_0} = 7{\cdot}10^{21}$ (m^{-3})) was prescribed as that used by Kuhl et al. (2005) for their transversely isotropic 8-chain model. In the absence of relevant shear experiments for rabbit skin, the constitutive parameters μ_1 and μ_2 were determined by the optimisation procedure but could have been determined by carrying out appropriate shear tests.

A possible approach to fully characterise the transversely isotropic material described in Section 3.2 would be to carry out a series of four tests that would effectively decouple the four kinematic modes of the constitutive formulation. A homogeneous compression test would characterise the parameter of the volumetric strain energy function (Eq. (59)). A pure shear in the plane of isotropy (orthogonal to the fibre direction) would be used to determine the shear modulus μ_1 (Eq. (61)). A pure shear along the fibre direction would characterise the fibre–fibre/matrix–fibre shear modulus μ_2 (Eq. (62)). A pure uniaxial extension along the fibre direction (stretch λ) would determine the fibre stress–strain curve from which the associated constitutive parameters could be deduced. The lateral contraction in the plane orthogonal to the fibre direction would characterise the ratio of the three principal stretches which is directly related to the volumetric invariant J:

$$J = \lambda_1\lambda_2\lambda. \tag{97}$$

The two (equal) lateral stretches $\lambda_1 = \lambda_2$ could be iteratively determined (using a Newton–Raphson method for example, see Bischoff et al., 2002a) by assuming traction-free conditions on the lateral sides of the sample and from Eq. (97) J would be determined.

For an orthotropic material such as skin, a uniaxial extension along the second family of fibres would characterise the associate constitutive parameters. However, it would have to be assumed that there is no direct mechanical coupling between the two families of fibres. The fibre–fibre/matrix–fibre shear modulus associated with the second family of fibres would be determined from a pure shear along the direction of these fibres. Tests based on biaxial extensions or multiaxial extensions (Kvistedal and Nielsen, 2009) could also be imagined to isolate more appropriately the respective contributions of each family of fibres.

Although the parameters a, b and $\bar{\lambda}_\beta^c$ were estimated directly from the locking stretches observed experimentally for both direction of anisotropy they could also have been determined via an optimisation procedure. Conversely, other constitutive parameters that were optimised could have been determined from physical measurements: contour length, persistence length, initial length. It is relevant to point out that the contour lengths of collagen molecules for both families of fibre were assumed to be identical whilst their initial and persistence length were allowed to be different. The entropic chain characteristics were found to be: $L_{n_0} \simeq 2.792$, $L_p^{n_0} \simeq 0.200$ and $r_{0n_0} \simeq 1.368$ for the first family of fibres (head-to-tail direction) while, for the second family of fibres they were: $L_{m_0} \simeq 2.792$, $L_p^{m_0} \simeq 0.591$ and $r_{0m_0} \simeq 1.741$. Human skin contains 80%–90% of type I collagen while the 20%/10% left consist mainly of type III collagen (Shimizu, 2007). The contour and persistence length of type I collagen molecules have been found to be respectively 14.5 ± 7.3 (nm) and 309 ± 41 (nm) by Sun et al. (2002). This was determined by fitting a worm-like chain elasticity model to the force–extension curve resulting from a direct tensile experiment of a type I collagen monomer using optical tweezers. In another study based on a similar experimental protocol, Sun et al. (2004) estimated the persistence length of type II collagen to be 11.2 ± 8.4 (nm). The persistence length of bovine skin collagen was found to be 57 and 40 nm for respectively type I and type III collagen molecules (Hofmann et al., 1984).

The contour and persistence length described in Section 3 have been normalised by the tropocollagen contour length.

This means that, if one assumes a 309 nm tropocollagen contour length for type I collagen, the persistence length (determined via numerical optimisation) for the families of fibre 1 and 2 are respectively about 22 and 65 nm. These figures lie within a similar range of what has been determined experimentally (Hofmann et al., 1984; Sun et al., 2001, 2002, 2004) and as a result of molecular dynamics simulations (Buehler and Wong, 2007; Gautieri et al., 2010). From the force–stretch curve of a single tropocollagen molecule and assuming a 301.7 nm contour length, Buehler and Wong (2007) deduced a 16 nm persistence length which correlates very well with experimental measurements using optical tweezers (Sun et al., 2002, 2004). Here, for the present study, it is important to point out that results of the optimisation are non-unique and different combinations of constitutive parameters could equally fit the experimental results. Experimental data should be used to refine the physical range of constitutive parameters. As highlighted by Kuhl et al. (2005) the ratio of the persistence length over the contour length is key in controlling the stiffness of the collagen assemblies and by modulating it one can obtain a good fit between the present theoretical model and the experimental data.

The stress response along the second family of fibres is under-estimated for stretches up to about 1.4 (a similar observation could be made by superimposing Fig. 5(a) and (b) of Kuhl et al.'s paper (2005)) while the response is over-estimated for stretches up to 1.8 in the case of the first family of fibres (head-to-tail direction).

Overall, the fit of the present constitutive model to the experimental data of (Lanir and Fung, 1972) is better than that obtained using a transversely isotropic worm-like chain model (Kuhl et al., 2005) which relies on network properties of a one family of fibres model to induce orthotropic properties.

A limitation of the present formulation is that mechanical coupling between the two families of fibres has not been accounted for *directly* but this could be remediated by introducing an appropriate coupling function that might, for example, couple the shear invariants of each respective family of fibres. In the constitutive model presented in this paper the coupling between fibre families is present via the mutual interactions that each family of fibres has with the matrix.

For the identification of the constitutive parameters it was assumed that the continuum composite material was nearly incompressible because biological soft tissues contain a large proportion of water. It is well known that internal hydration conditions significantly affect the mechanical properties of biological tissues such as skin (Jemec and Serup, 1990). Intuitively, one would expect that reducing water content would means that the diminished role of water molecules around collagen molecules and microfibrils would have important direct nanotribological effects on their mechanics as well as on the overall macroscopic mechanical behaviour of the tissue. However, the exact multi-scale mechanisms underlying these phenomena remain unclear. In a recent study, Gautieri et al. (2011) developed the first experimentally validated model of s collagen microfibril incorporating the full biochemical details of the amino acid sequence of associated molecules whilst also accounting for their correct structural arrangement at the nanoscale. By simulating a tensile test on a microfibril these authors showed that hydrated and dehydrated collagen microfibrils have very distinct mechanical behaviours. It was found that hydrated collagen microfibrils exhibit two different deformation regimes. Under moderately low strain (<10%) the predicted Young's modulus of the microfibril is about 300 MPa whilst this value increased to about 1.2 GPa (four-fold increase) for large strains (>10%). This non-linear behaviour is in stark contrast with the mostly linear variation of the predicted Young's modulus for dehydrated collagen microfibrils which was found to vary between 1.8 and 2.25 GPa (for strains greater than 10%). These computational results corroborate experimental results which highlighted a nine-fold increase of collagen fibril stiffness for dehydrated versus hydrated states (van der Rijt et al., 2006). Gautieri et al.'s study (2011) demonstrated that collagen microfibrils display a rich set of deformation modes originating from the complex interplay of the deformation mechanisms associated with each length scale and the combined effects of the hierarchical structural arrangement. The stiffness of entropic molecular chains can be estimated by using the simple following formula (Buehler, 2008b):

$$L_p = \frac{EI}{\hat{\kappa}\theta} \tag{98}$$

where EI represents the bending stiffness of the chain. By assuming that the molecular chain is contained within a cylindrical volume of radius R and that it exhibits homogeneous structural properties, the Young's modulus of the molecular chain can be deduced (Gautieri et al., 2010; Landau and Lifshitz, 1986):

$$E = \frac{4L_p\hat{\kappa}\theta}{\pi R^4}. \tag{99}$$

Based on Eq. (99), if one assumes a molecular radius of 0.8 nm and considering the identified persistence lengths for the families of Type I collagen fibre 1 and 2 – respectively 22 and 65 nm – one obtains equivalent Young's modulus of 293 and 865 MPa. These values lie within one order of magnitude less of what has been determined experimentally and through computational modelling studies (see Fig. 5 and Table 1 in Gautieri et al. (2011)). However, using Eq. (99), Sun et al. (2002) estimated the Young's modulus of collagen molecules to range between 350 MPa and 12 GPa. Fig. 5 represents the variation of a tropocollagen molecule Young's modulus as a function of its molecular radius and persistence length. As pointed out by Gautieri et al. (2010), the predictive relationship (99) might not be valid and this could be explained by the lack of structural homogeneity of the collagen molecule.

In the same way that the macroscopic stiffness of collagenous tissues is much lower than that of individual collagen fibrils and microfibrils because of length scale effects, the Young's modulus of microfibrils is significantly lower than that of individual tropocollagen molecules. Table 1 in Gautieri et al. (2011) reports averaged values of equivalent Young's modulus (between various experimental and computational studies) of 4.8 ± 2.0 GPa, 0.6 ± 0.2 GPa and 3.26 GPa for respectively individual collagen molecules, wet collagen microfibrils and dry collagen microfibrils. Results of

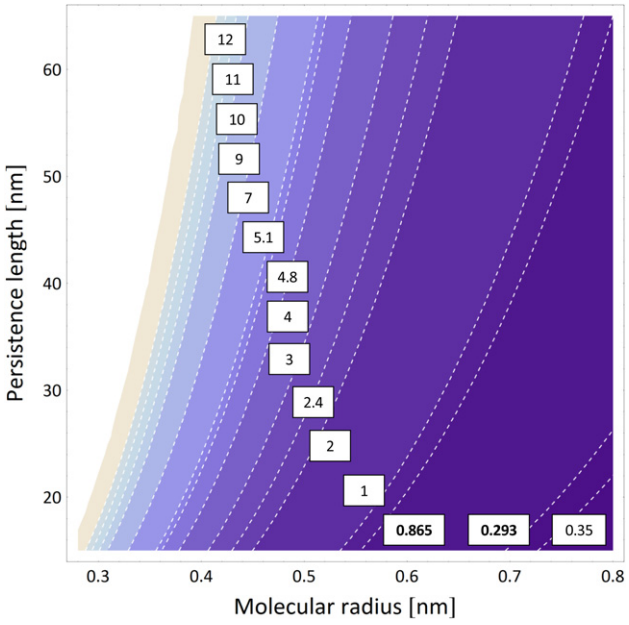

Fig. 5 – Predicted Young's modulus (GPa) of a tropocollagen molecule as a function of its persistence length (nm) and molecular radius (nm) (Eq. (99)). Key values of Young's modulus found in the literature are featured as isocontours: 0.35–12 GPa (Sun et al., 2002), 2.4 GPa (Vesentini et al., 2005), 3 GPa (Sasaki and Odajima, 1996a), 4 GPa (Gautieri et al., 2009a, 2010), 4.8 GPa (Lorenzo and Caffarena, 2005), 5.1 GPa (Cusack and Miller, 1979), 7 GPa (Buehler, 2006a), 9 GPa (Harley et al., 1977). The values 0.293 and 0.865 GPa correspond to a persistence length of respectively 22 and 65 nm (molecular radius = 0.8 nm). These two persistence lengths were obtained as a result of parameter identification (see Section 6.1).

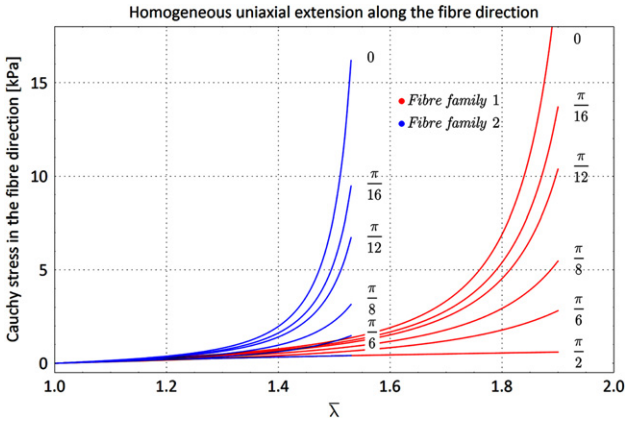

Fig. 6 – Influence of the fibre angle on the Cauchy stress along each fibre direction.

Ramachandran analyses carried out by Gautieri et al. (2011) seem to indicate that the loss of water around microfibrils lead to a structural break down at the molecular scale which results in the observed stress hardening. When a micro/nanofibril is stretched, the potential lubricating-like role of water molecules delays the onset of shear interactions between tropocollagen assemblies by leading to structural rearrangement at the nanofibril level, i.e. slippage rather than elongation (Gautieri et al., 2009b). Naturally, there are other types of complex coupled physico-chemical phenomena involved in these nanoscale interactions.

Physically, at the macroscopic level, the reduction of water would affect the ability of the tissue to resist compressive loads. It is likely that collagen fibres will experience more severe bending deformations because of the stronger coupling between macroscopic and mesoscopic deformations and the reduced dominance of bulk properties of the matrix over its shear properties.

For the proposed constitutive model, if the bulk compressibility of the matrix of the continuum composite is increased, for example as a result of a loss of water, any tension exerted at the macroscopic level is likely to have a more localised effect by minimising the transverse (with respect to the loading axis) bending recruitment of collagen fibres because of the relaxed constraint of incompressibility which has non-local effects. It must be pointed out that the constitutive formulation considers that collagen fibres are incompressible. By the very statistical nature of the worm-like chain model every family of collagen fibres is assumed to have a statistical distribution with zero variance around a mean direction. This implies that any mechanical solicitation of the macroscopic tissue that is not aligned with any (local) fibre direction is bound to be (locally) transmitted only by the shear interactions between the fibres and the matrix and the shear and tensile deformation of the matrix.

At the moment, the link between the hydration state of microfibrils and the magnitude and evolution of their homogenised stiffness highlighted by Gautieri et al. (2011) is not accounted for in the present structurally-based continuum formulation. This could be achieved by, for example, introducing an anisotropic shear energy function $\hat{\psi}^2$ coupling the volumetric invariant J and the anisotropic shear invariant α_2. However, this is left for future work.

6.2. *Influence of the fibre direction*

Results of the parametric evaluation of the Cauchy stress in the initial fibre orientations (along the directions aligned with the *original* unit vectors $\boldsymbol{n}_0$ and $\boldsymbol{m}_0$, that is **X** and **Y**, see Fig. 2) are presented for both fibre directions on Fig. 6. By construction, the Cauchy stress in any of the two fibre directions vanishes when the angle between the principal stretching directions and their respective initial fibre unit vectors reaches 90°. Increasing these angles from 0° to 90° around the Z-axis (direction **Z**) has the effect of decreasing the locking stretch and therefore making the tissue more compliant in the corresponding fibre direction. The fibre stress responses are very sensitive to the load directions. For example, rotating $\boldsymbol{n}_0$ by 15° around the direction **Z** leads to a reduction on the Cauchy stress along the original direction $\boldsymbol{n}_0$ by more than 50%. This equally applies to a 15° rotation of $\boldsymbol{m}_0$. Results showed the key influence of fibre orientation on the mechanical response of the tissue under simulated homogeneous extension.

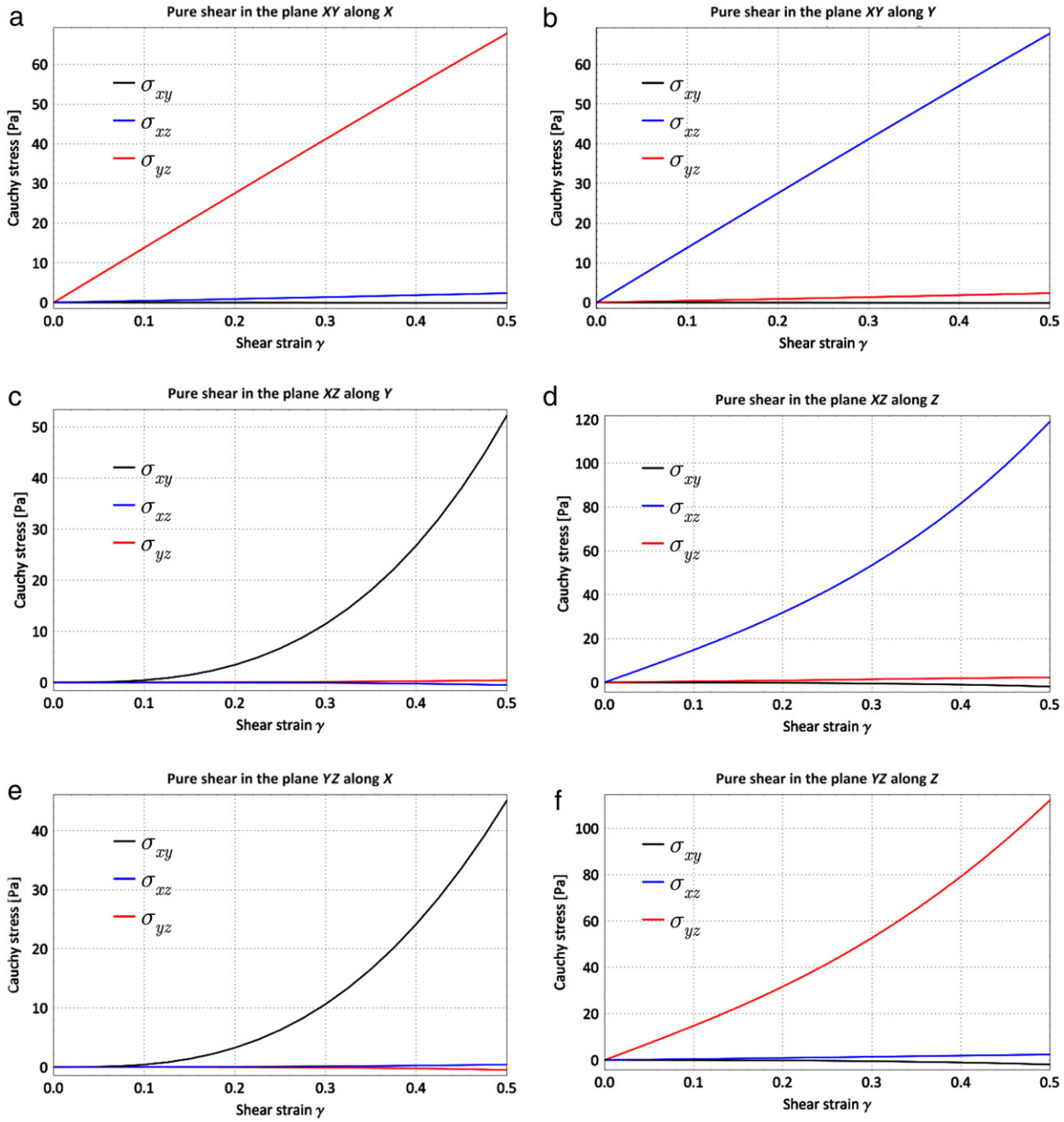

Fig. 7 – Plots of the shear stress σ_{xy}, σ_{xz} and σ_{yz} as a function of the shear strain γ for the six shear modes considered.

6.3. *Simple shear stress response for the 6 shear modes*

The evolution of the three shear components of the Cauchy stress tensor as a function of the shear strain are reported for each of the six shear modes (Table 3) on Fig. 7. The directions **X** and **Y** corresponds respectively to the head-to-tail direction (fibre family 1) and the direction orthogonal to it (fibre family 2).

This means that the fibre–fibre and fibre–matrix shear interactions are associated with the shear components of the Cauchy stress tensor σ_{xz} and σ_{yz} while the isotropic matrix shear interactions are represented by σ_{xy}. For shear modes 1 and 2 the shear stresses vary linearly as a function of the shear strain. As expected σ_{xy} vanishes while σ_{yz} and σ_{xz} dominate respectively for the first and second shear modes. For shear modes 3 and 5, σ_{xy}, the dominant (positive) shear stress, exhibits a parabolic evolution while a (negative) slightly non-linear evolution is observed for shear modes 4 and 6 which, in absolute value is significantly less than respectively σ_{xz} and σ_{yz} (also featuring a non-linear evolution).

For shear modes 3 and 4 σ_{yz} is null while σ_{xz} vanishes for shear modes 5 and 6. Functional forms for the shear energies will have to be based on more concrete data from appropriate experiments but it was shown that, in principle, any shear behaviour can be accounted for in the present formulation.

6.4. *Sensitivity of the shear response for an indentation test*

The contour plots of the 3 shear stress components and their associated parameter sensitivities are reported on Fig. 8 (σ_{xy}), Fig. 9 (σ_{xz}) and Fig. 10 (σ_{yz}). The sensitivities are reported with respect to the 3 shear moduli featured in the constitutive model (μ_0, μ_1 and μ_2) and the fibre deviation angles (Eq. (95)). In the two previous series of analyses it was assumed that collagen fibres had a negligible compressive and bending stiffness. This is an assumption often made when formulating constitutive laws for biological soft tissues (Holzapfel et al., 2000; Limbert et al., 2003; Weiss et al., 1996) because collagenous structures buckle under very small compressive loads. This effectively means that collagen fibres have no stiffness when their initial length is reduced. To assess the effect of this assumption on the shear stress the sensitivities $\partial\sigma_{xy}/\partial\mu_0$, $\partial\sigma_{xz}/\partial\mu_0$ and $\partial\sigma_{yz}/\partial\mu_0$ were calculated. Quantitatively, the effect is small but this not the case in terms of spatial distribution.

The maximum magnitude of shear stress were 137, 237 and 267 Pa respectively for σ_{xy}, σ_{xz} and σ_{yz} (Figs. 8–10). As discussed in Section 5.3, each sensitivity value determines how much change is observed in the response variable as a result of a unit change in the corresponding parameter. For example, $\partial\sigma_{xy}/\partial\mu_0$ quantifies by how much σ_{xy} will change if μ_0 is increased by one unit of μ_0; in that case, by 1 Pa. Figs. 8–10 highlight the complex spatial dependency of the three shear stresses on the three shear moduli and the collagen fibre directions in the case of a simple vertical indentation experiment. Because of the symmetry of the problem, the spatial sensitivity on the shear moduli is centrally symmetric with a 180° period while the spatial sensitivity on the fibre orientation angles is symmetric with respect to two mutually orthogonal vertical planes, intersecting at the centre of the sample and perpendicular to the plane spanned by $\mathbf{X}$ and $\mathbf{Y}$.

As expected, the sensitivities $\partial\sigma_{xy}/\partial\theta_x(\boldsymbol{n}_0)$, $\partial\sigma_{xy}/\partial\theta_y(\boldsymbol{m}_0)$, $\partial\sigma_{xz}/\partial\theta_x(\boldsymbol{n}_0)$, $\partial\sigma_{xz}/\partial\theta_y(\boldsymbol{m}_0)$, $\partial\sigma_{yz}/\partial\theta_x(\boldsymbol{n}_0)$, $\partial\sigma_{yz}/\partial\theta_y(\boldsymbol{m}_0)$ were null and therefore were not plotted on Figs. 8–10.

Overall, the shear parameters and fibre vectors have a complex influence on the spatial distribution of shear stresses during a simulated indentation tests and this is an important result as it highlights the fact that constitutive models based on these input variables have the ability to capture specific mechanical responses.

7. Conclusion

A novel mesoscopically-based continuum constitutive framework for transversely isotropic and orthotropic biological soft tissues was developed. One of the key features of the constitutive formulation is the ability to decouple volumetric, deviatoric stretch(es) in the fibre direction(s), cross-fibre shear and fibre-to-fibre/matrix-to-fibre shear stress responses. This allows to link directly constitutive parameters to the particular mechanical mode considered provided suitable physical experiments are conducted. Another important attractive feature of the constitutive equations is that the collagen fibre response is based on physical geometrical/structural parameters (e.g. contour/persistence lengths) that can be measured experimentally or determined *ab initio* from molecular dynamic simulations. The orthotropic hyperelastic model was shown to reproduce very well the experimental multi-axial properties of rabbit skin whilst providing a new insight into the shear response of a skin sample subjected to a simulated indentation test.

Acknowledgements

Financial support from the Engineering and Physical Sciences Research Council (EPSRC) [Grant EP/F034296/1] and the University of Southampton is gratefully acknowledged.

Appendix A. Kronecker product of second order tensors

The Kronecker product of two second order tensors (Schafer, 1996) is defined by:

$$(\mathbf{A}\boxtimes\mathbf{B})_{\alpha\beta} = (\mathbf{A})_{ij}(\mathbf{B})_{kl} \quad \text{where} \quad \begin{cases}\alpha = p(i-1)+k\\ \beta = q(j-1)+l\end{cases}$$
$$\forall\, \mathbf{A}_{m\times n}, \mathbf{B}_{p\times q} \text{ second-order tensors} \tag{A.1}$$

$\mathbf{A}\boxtimes\mathbf{B}$ is a $mp\times nq$ second-order tensor.

Example 1. Let us consider the matrix representations of two arbitrary tensors $\mathbf{A}$ and $\mathbf{B}$ (the matrix representation of a tensor $\mathbf{T}$ is denoted by $[\mathbf{T}]$):

$$[\mathbf{A}] = \begin{bmatrix} A_{11} & A_{12}\\ A_{21} & A_{22}\end{bmatrix}; \qquad [\mathbf{B}] = \begin{bmatrix} B_{11} & B_{12}\\ B_{21} & B_{22}\\ B_{31} & B_{32}\end{bmatrix}.$$

The Kronecker product of $\mathbf{A}$ and $\mathbf{B}$, $\mathbf{A}\boxtimes\mathbf{B}$ is given by:

$$[\mathbf{A}\boxtimes\mathbf{B}] = \begin{bmatrix} \begin{bmatrix} A_{11}B_{11} & A_{11}B_{12}\\ A_{11}B_{21} & A_{11}B_{22}\\ A_{11}B_{31} & A_{11}B_{32}\end{bmatrix} & \begin{bmatrix} A_{12}B_{11} & A_{12}B_{12}\\ A_{12}B_{21} & A_{12}B_{22}\\ A_{12}B_{31} & A_{12}B_{32}\end{bmatrix}\\ \begin{bmatrix} A_{21}B_{11} & A_{21}B_{12}\\ A_{21}B_{21} & A_{21}B_{22}\\ A_{21}B_{31} & A_{21}B_{32}\end{bmatrix} & \begin{bmatrix} A_{22}B_{11} & A_{22}B_{12}\\ A_{22}B_{21} & A_{22}B_{22}\\ A_{22}B_{31} & A_{22}B_{32}\end{bmatrix}\end{bmatrix}. \tag{A.2}$$

Example 2. The tensors $\boldsymbol{\Lambda}\otimes\boldsymbol{\Lambda}$, $\mathbf{I}\boxtimes\boldsymbol{\Lambda}$ and $\boldsymbol{\Lambda}\boxtimes\mathbf{I}$ are used to calculate the stress projection tensor $\mathbb{P}^{\hat{\boldsymbol{\sigma}}^1}$ (see Eq. (20)). The unit vector in the spatial configuration is $\boldsymbol{n} = \{n_1, n_2, n_3\}$ and the corresponding structural tensor is $\boldsymbol{\Lambda} = \boldsymbol{n}\otimes\boldsymbol{n}$.

See Eqs. (A.3)–(A.6) given in Box I.

Appendix B. Integrity bases of stress tensors

The integrity bases of the transversely isotropic symmetry group in the material configuration are:

$$\mathfrak{B}_1^{\mathbf{S}} = \frac{1}{2}J\mathbf{C}^{-1} \tag{B.1}$$

$$\mathfrak{B}_2^{\mathbf{S}} = -\frac{1}{6}\bar{\lambda}\mathbf{C}^{-1} + \frac{1}{2\bar{\lambda}}J^{-\frac{2}{3}}\boldsymbol{\Lambda}_0 \tag{B.2}$$

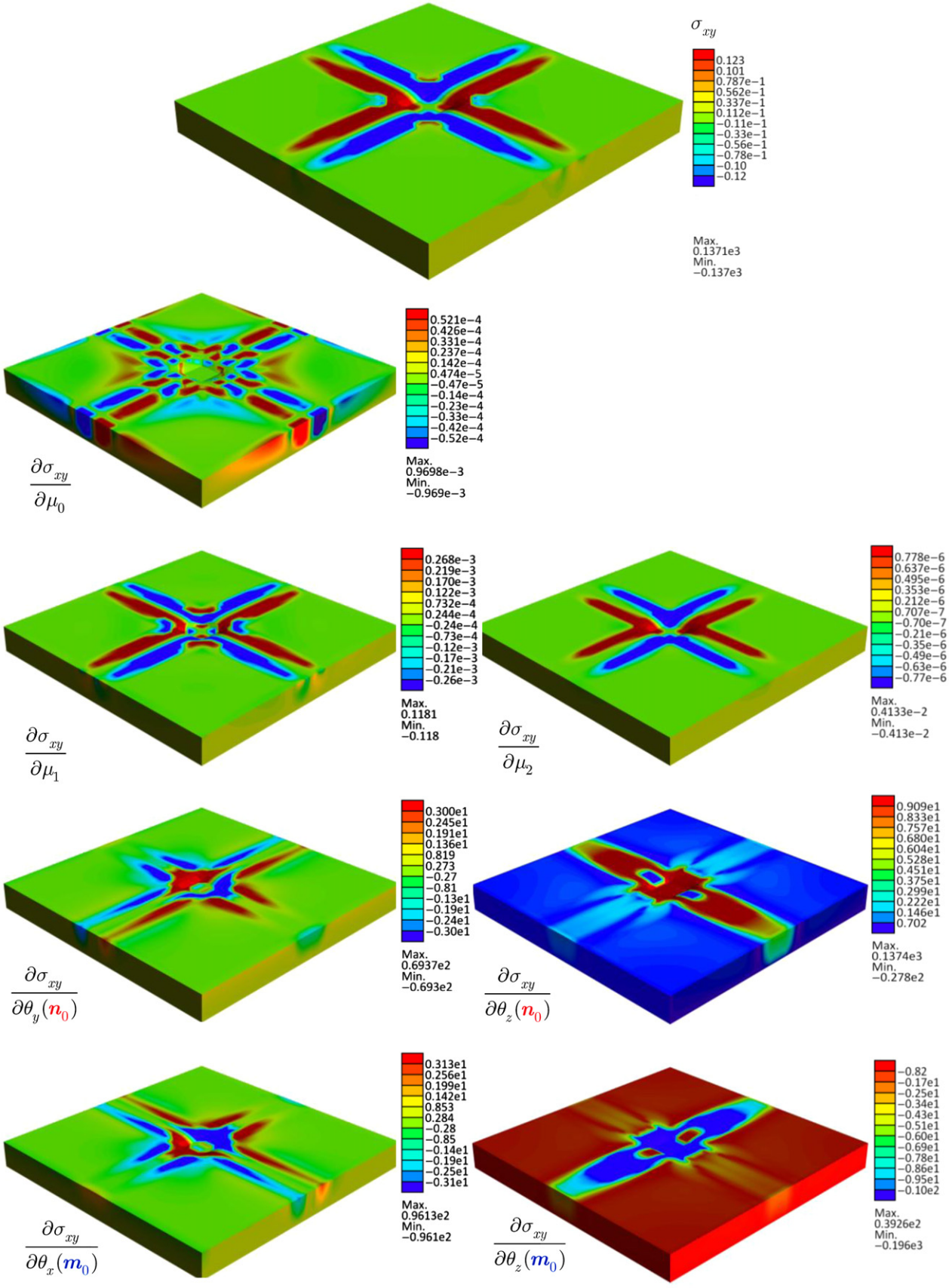

Fig. 8 – Shear stress σ_{xy} and its sensitivities with respect to a selected subset of the constitutive parameters and the direction of the fibre families.

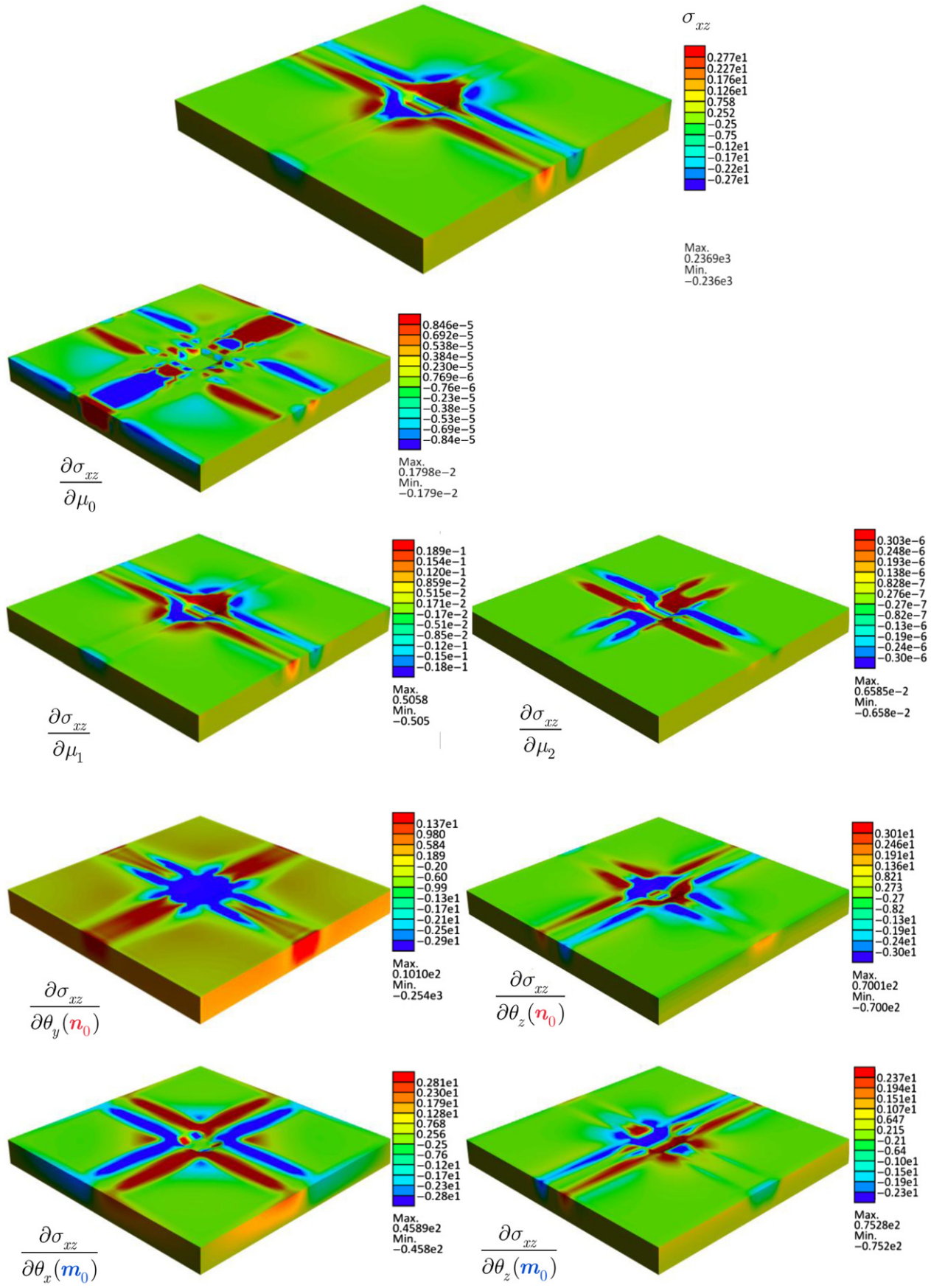

Fig. 9 – Shear stress σ_{xz} and its sensitivities with respect to a selected subset of the constitutive parameters and the direction of the fibre families.

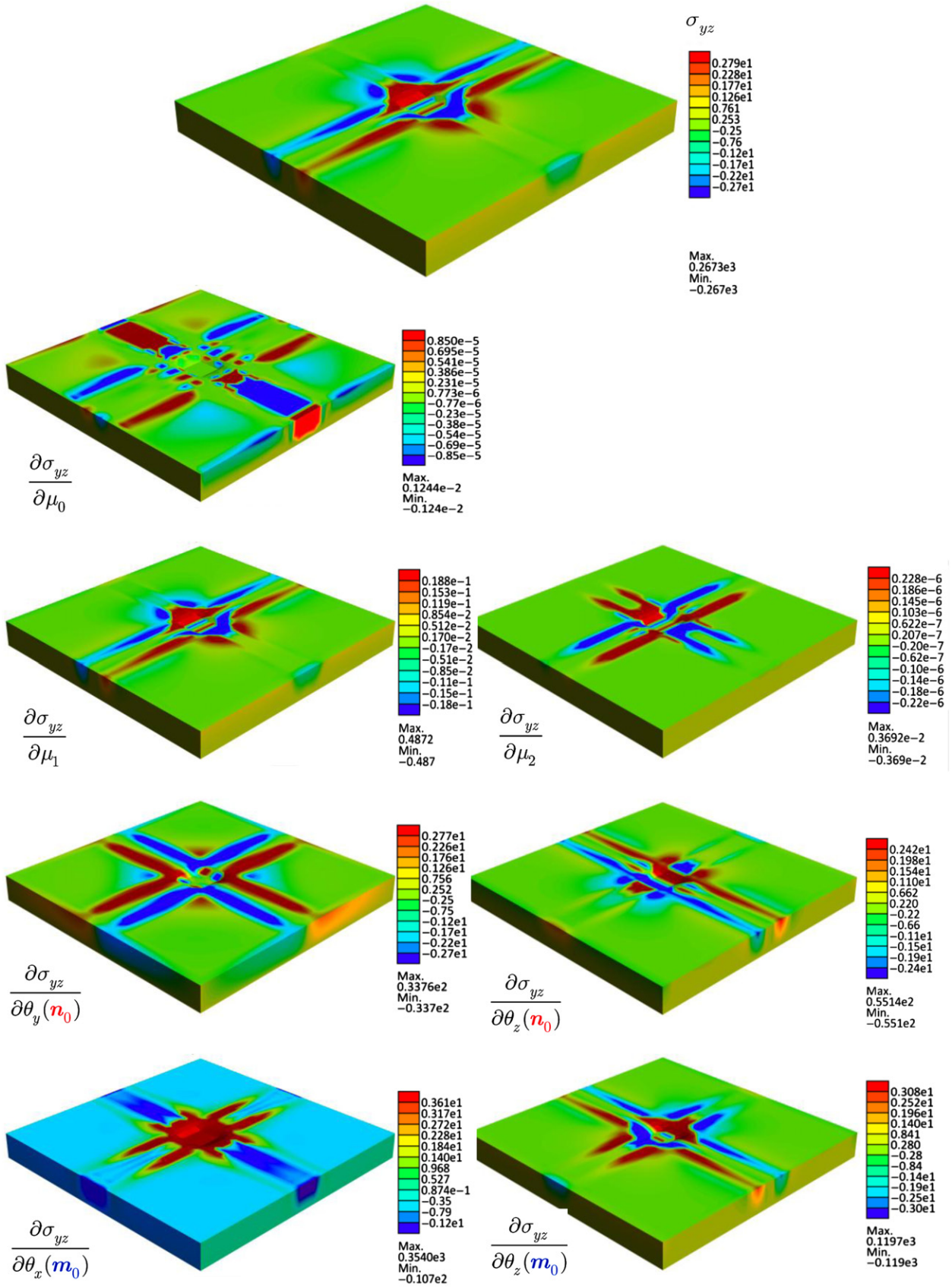

Fig. 10 – Shear stress σ_{yz} and its sensitivities with respect to a selected subset of the constitutive parameters and the direction of the fibre families.

$$[\mathbf{I}] = \begin{bmatrix} 1 & 0 & 0 \\ 0 & 1 & 0 \\ 0 & 0 & 1 \end{bmatrix}; \qquad [\mathbf{\Lambda}] = \begin{bmatrix} n_1^2 & n_1 n_2 & n_1 n_3 \\ n_1 n_2 & n_2^2 & n_2 n_3 \\ n_1 n_3 & n_2 n_3 & n_3^2 \end{bmatrix} \tag{A.3}$$

$$[\mathbf{\Lambda} \boxtimes \mathbf{\Lambda}] = \begin{bmatrix} \begin{bmatrix} n_1^4 & n_1^3 n_2 & n_1^3 n_3 \\ n_1^3 n_2 & n_1^2 n_2^2 & n_1^2 n_2 n_3 \\ n_1^3 n_3 & n_1^2 n_2 n_3 & n_1^2 n_3^2 \end{bmatrix} & \begin{bmatrix} n_1^3 n_2 & n_1^2 n_2^2 & n_1^2 n_2 n_3 \\ n_1^2 n_2^2 & n_1 n_2^3 & n_1 n_2^2 n_3 \\ n_1^2 n_2 n_3 & n_1 n_2^2 n_3 & n_1 n_2 n_3^2 \end{bmatrix} & \begin{bmatrix} n_1^3 n_3 & n_1^2 n_2 n_3 & n_1^2 n_3^2 \\ n_1^2 n_2 n_3 & n_1 n_2^2 n_3 & n_1 n_2 n_3^2 \\ n_1^2 n_3^2 & n_1 n_2 n_3^2 & n_1 n_3^3 \end{bmatrix} \\ \begin{bmatrix} n_1^3 n_2 & n_1^2 n_2^2 & n_1^2 n_2 n_3 \\ n_1^2 n_2^2 & n_1 n_2^3 & n_1 n_2^2 n_3 \\ n_1^2 n_2 n_3 & n_1 n_2^2 n_3 & n_1 n_2 n_3^2 \end{bmatrix} & \begin{bmatrix} n_1^2 n_2^2 & n_1 n_2^3 & n_1 n_2^2 n_3 \\ n_1 n_2^3 & n_2^4 & n_2^3 n_3 \\ n_1 n_2^2 n_3 & n_2^3 n_3 & n_2^2 n_3^2 \end{bmatrix} & \begin{bmatrix} n_1^2 n_2 n_3 & n_1 n_2^2 n_3 & n_1 n_2 n_3^2 \\ n_1 n_2^2 n_3 & n_2^3 n_3 & n_2^2 n_3^2 \\ n_1 n_2 n_3^2 & n_2^2 n_3^2 & n_2 n_3^3 \end{bmatrix} \\ \begin{bmatrix} n_1^3 n_3 & n_1^2 n_2 n_3 & n_1^2 n_3^2 \\ n_1^2 n_2 n_3 & n_1 n_2^2 n_3 & n_1 n_2 n_3^2 \\ n_1^2 n_3^2 & n_1 n_2 n_3^2 & n_1 n_3^3 \end{bmatrix} & \begin{bmatrix} n_1^2 n_2 n_3 & n_1 n_2^2 n_3 & n_1 n_2 n_3^2 \\ n_1 n_2^2 n_3 & n_2^3 n_3 & n_2^2 n_3^2 \\ n_1 n_2 n_3^2 & n_2^2 n_3^2 & n_2 n_3^3 \end{bmatrix} & \begin{bmatrix} n_1^2 n_3^2 & n_1 n_2 n_3^2 & n_1 n_3^3 \\ n_1 n_2 n_3^2 & n_2^2 n_3^2 & n_2 n_3^3 \\ n_1 n_3^3 & n_2 n_3^3 & n_3^4 \end{bmatrix} \end{bmatrix} \tag{A.4}$$

$$[\mathbf{I} \boxtimes \mathbf{\Lambda}] = \begin{bmatrix} \begin{bmatrix} n_1^2 & n_1 n_2 & n_1 n_3 \\ n_1 n_2 & n_2^2 & n_2 n_3 \\ n_1 n_3 & n_2 n_3 & n_3^2 \end{bmatrix} & \begin{bmatrix} 0 & 0 & 0 \\ 0 & 0 & 0 \\ 0 & 0 & 0 \end{bmatrix} & \begin{bmatrix} 0 & 0 & 0 \\ 0 & 0 & 0 \\ 0 & 0 & 0 \end{bmatrix} \\ \begin{bmatrix} 0 & 0 & 0 \\ 0 & 0 & 0 \\ 0 & 0 & 0 \end{bmatrix} & \begin{bmatrix} n_1^2 & n_1 n_2 & n_1 n_3 \\ n_1 n_2 & n_2^2 & n_2 n_3 \\ n_1 n_3 & n_2 n_3 & n_3^2 \end{bmatrix} & \begin{bmatrix} 0 & 0 & 0 \\ 0 & 0 & 0 \\ 0 & 0 & 0 \end{bmatrix} \\ \begin{bmatrix} 0 & 0 & 0 \\ 0 & 0 & 0 \\ 0 & 0 & 0 \end{bmatrix} & \begin{bmatrix} 0 & 0 & 0 \\ 0 & 0 & 0 \\ 0 & 0 & 0 \end{bmatrix} & \begin{bmatrix} n_1^2 & n_1 n_2 & n_1 n_3 \\ n_1 n_2 & n_2^2 & n_2 n_3 \\ n_1 n_3 & n_2 n_3 & n_3^2 \end{bmatrix} \end{bmatrix} \tag{A.5}$$

$$[\mathbf{\Lambda} \boxtimes \mathbf{I}] = \begin{bmatrix} \begin{bmatrix} n_1^2 & 0 & 0 \\ 0 & n_1^2 & 0 \\ 0 & 0 & n_1^2 \end{bmatrix} & \begin{bmatrix} n_1 n_2 & 0 & 0 \\ 0 & n_1 n_2 & 0 \\ 0 & 0 & n_1 n_2 \end{bmatrix} & \begin{bmatrix} n_1 n_3 & 0 & 0 \\ 0 & n_1 n_3 & 0 \\ 0 & 0 & n_1 n_3 \end{bmatrix} \\ \begin{bmatrix} n_1 n_2 & 0 & 0 \\ 0 & n_1 n_2 & 0 \\ 0 & 0 & n_1 n_2 \end{bmatrix} & \begin{bmatrix} n_2^2 & 0 & 0 \\ 0 & n_2^2 & 0 \\ 0 & 0 & n_2^2 \end{bmatrix} & \begin{bmatrix} n_2 n_3 & 0 & 0 \\ 0 & n_2 n_3 & 0 \\ 0 & 0 & n_2 n_3 \end{bmatrix} \\ \begin{bmatrix} n_1 n_3 & 0 & 0 \\ 0 & n_1 n_3 & 0 \\ 0 & 0 & n_1 n_3 \end{bmatrix} & \begin{bmatrix} n_2 n_3 & 0 & 0 \\ 0 & n_2 n_3 & 0 \\ 0 & 0 & n_2 n_3 \end{bmatrix} & \begin{bmatrix} n_3^2 & 0 & 0 \\ 0 & n_3^2 & 0 \\ 0 & 0 & n_3^2 \end{bmatrix} \end{bmatrix} \tag{A.6}$$

Box I.

$$\mathfrak{B}_3^{\mathbf{S}} = \left(J^{-\frac{4}{3}} I_5 - J^{-\frac{2}{3}} I_1\right) \mathbf{C}^{-1} + \left(\frac{J^{-\frac{4}{3}}}{\bar{\lambda}} I_1 + \frac{2-\bar{\lambda}}{2\bar{\lambda}^3} J^{-\frac{5}{3}} I_5\right) \mathbf{\Lambda}_0 + \frac{J^{-\frac{4}{3}}}{\bar{\lambda}} \left(\boldsymbol{n}_0 \otimes \mathbf{C}\boldsymbol{n}_0 + \boldsymbol{n}_0 C \otimes \boldsymbol{n}_0\right) \tag{B.3}$$

$$\mathfrak{B}_4^{\mathbf{S}} = -\frac{2}{J^2 \bar{\lambda}^6} \mathbf{\Lambda}_0 + \frac{J^{-\frac{2}{3}}}{\bar{\lambda}^4} \left(\boldsymbol{n}_0 \otimes \mathbf{C}\boldsymbol{n}_0 + \boldsymbol{n}_0 \mathbf{C} \otimes \boldsymbol{n}_0\right). \tag{B.4}$$

The integrity bases of the transversely isotropic symmetry group in the spatial configuration are:

$$\mathfrak{B}_1^{\sigma} = \frac{1}{2} J \mathbf{I} \tag{B.5}$$

$$\mathfrak{B}_2^{\sigma} = -\frac{1}{6} \bar{\lambda} \mathbf{I} + \frac{J^{\frac{1}{3}}}{2} \bar{\lambda} \boldsymbol{n} \otimes \boldsymbol{n} \tag{B.6}$$

$$\mathfrak{B}_3^{\sigma} = \left(J^{-\frac{4}{3}} I_5 - J^{-\frac{2}{3}} I_1\right) \mathbf{I} + \left(\frac{J^{-\frac{2}{3}}}{2} I_1 \bar{\lambda} + \frac{2-\bar{\lambda}}{2\bar{\lambda}^2} J^{-1} I_5\right) \mathbf{\Lambda} + J^{-\frac{2}{3}} \bar{\lambda} \left(\boldsymbol{n} \otimes \mathbf{b}\boldsymbol{n} + \boldsymbol{n}\mathbf{b} \otimes \boldsymbol{n}\right) \tag{B.7}$$

$$\mathfrak{B}_4^{\sigma} = -\frac{2J^{-\frac{2}{3}}}{\bar{\lambda}^4} \mathbf{\Lambda} + \frac{1}{\bar{\lambda}^2} \left(\boldsymbol{n} \otimes \mathbf{b}\boldsymbol{n} + \boldsymbol{n}\mathbf{b} \otimes \boldsymbol{n}\right). \tag{B.8}$$

REFERENCES

Arruda, E.M., Boyce, M.C., 1993. A three-dimensional constitutive model for the large stretch behavior of rubber elastic-materials. Journal of the Mechanics and Physics of Solids 41, 389–412.

Bass, E.C., Ashford, F.A., Segal, M.R., Lotz, J.C., 2004. Biaxial testing of human annulus fibrosus and its implications for a constitutive formulation. Annals of Biomedical Engineering 32, 1231–1242.

Bischoff, J.E., Arruda, E.M., Grosh, K., 2000. Finite element modeling of human skin using an isotropic, nonlinear elastic constitutive model. Journal of Biomechanics 33, 645–652.

Bischoff, J.E., Arruda, E.M., Grosh, K., 2002a. Finite element simulations of orthotropic hyperelasticity. Finite Elements in Analysis and Design 38, 983–998.

Bischoff, J.E., Arruda, E.M., Grosh, K., 2002b. Orthotropic hyperelasticity in terms of an arbitrary molecular chain model. Journal of Applied Mechanics, Transactions of the ASME 69, 198–201.

Blemker, S.S., Pinsky, P.M., Delp, S.L., 2005. A 3D model of muscle reveals the causes of nonuniform strains in the biceps brachii. Journal of Biomechanics 38, 657–665.

Boehler, 1978. Lois de comportement anisotrope des milieux continus. Journal de Mécanique 17, 153–190.
Buehler, M.J., 2006a. Atomistic and continuum modeling of mechanical properties of collagen: elasticity, fracture, and self-assembly. Journal of Materials Research 21, 1947–1961.
Buehler, M.J., 2006b. Nature designs tough collagen: explaining the nanostructure of collagen fibrils. Proceedings of the National Academy of Sciences of the United States of America 103, 12285–12290.
Buehler, M., 2008a. Hierarchical nanomechanics of collagen fibrils: atomistic and molecular modeling. In: Fratzl, P. (Ed.), Collagen: Structure and Mechanics. Springer Science, New York, pp. 175–247.
Buehler, M.J., 2008b. 4 atomistic elasticity: linking atoms and continuum. In: Atomistic Modeling of Materials Failure. Springer, New York, p. 151.
Buehler, M.J., 2008c. Molecular architecture of collagen fibrils: a critical length scale for tough fibrils. Current Applied Physics 8, 440–442.
Buehler, M.J., 2008d. Nanomechanics of collagen fibrils under varying cross-link densities: atomistic and continuum studies. Journal of the Mechanical Behavior of Biomedical Materials 1, 59–67.
Buehler, M.J., Wong, S.Y., 2007. Entropic elasticity controls nanomechanics of single tropocollagen molecules. Biophysical Journal 93, 37–43.
Criscione, J.C., Douglas, A.S., Hunter, W.C., 2001. Physically based strain invariant set for materials exhibiting transversely isotropic behavior. Journal of the Mechanics and Physics of Solids 49, 871–897.
Criscione, J.C., Hunter, W.C., 2003. Kinematics and elasticity framework for materials with two fiber families. Continuum Mechanics and Thermodynamics 15, 613–628.
Criscione, J.C., McCulloch, A.D., Hunter, W.C., 2002. Constitutive framework optimized for myocardium and other high-strain, laminar materials with one fiber family. Journal of the Mechanics and Physics of Solids 50, 1681–1702.
Cusack, S., Miller, A., 1979. Determination of the elastic constants of collagen by Brillouin light scattering. Journal of Molecular Biology 135, 39–51.
Delalleau, A., Josse, G., Lagarde, J.M., Zahouani, H., Bergheau, J.M., 2006. Characterization of the mechanical properties of skin by inverse analysis combined with the indentation test. Journal of Biomechanics 39, 1603–1610.
Flory, P.J., 1969. Statistical Mechanics of Chain Molecules. John Wiley & Sons, Chichester, New York.
Flynn, C., McCormack, B.A.O., 2008. Finite element modelling of forearm skin wrinkling. Skin Research and Technology 14, 261–269.
Flynn, C.O., McCormack, B.A.O., 2009. A three-layer model of skin and its application in simulating wrinkling. Computer Methods in Biomechanics and Biomedical Engineering 12, 125–134.
Fratzl, P., 2008. Collagen: Structure and Mechanics. Springer.
Fung, Y.C., 1981. Biomechanics: Mechanical Properties of Living Tissues. Springer-Verlag, New York.
Fujita, Y., Wagner, D.R., Biviji, A.A., Duncan, N.A., Lotz, J.C., 2000. Anisotropic shear behavior of the annulus fibrosus: effect of harvest site and tissue prestrain. Medical Engineering & Physics 22, 349–357.
Garikipati, K., Arruda, E.M., Grosh, K., Narayanan, H., Calve, S., 2004. A continuum treatment of growth in biological tissue: the coupling of mass transport and mechanics. Journal of the Mechanics and Physics of Solids 52, 1595–1625.
Garikipati, K., Olberding, J.E., Narayanan, H., Arruda, E.M., Grosh, K., Calve, S., 2006. Biological remodelling: stationary energy, configuration change, internal variables and dissipation. Journal of the Mechanics and Physics of Solids 54, 1493–1515.
Gautieri, A., Buehler, M.J., Redaelli, A., 2009a. Deformation rate controls elasticity and unfolding pathway of single tropocollagen molecules. Journal of the Mechanical Behavior of Biomedical Materials 2, 130–137.
Gautieri, A., Vesentini, S., Redaelli, A., Buehler, M.J., 2009b. Intermolecular slip mechanism in tropocollagen nanofibrils. International Journal of Materials Research 100, 921–925.
Gautieri, A., Russo, A., Vesentini, S., Redaelli, A., Buehler, M.J., 2010. Coarse-grained model of collagen molecules using an extended martini force field. Journal of Chemical Theory and Computation 6, 1210–1218.
Gautieri, A., Vesentini, S., Redaelli, A., Buehler, M.J., 2011. Hierarchical structure and nanomechanics of collagen microfibrils from the atomic scale up. Nano Letters 11, 757–766.
Guo, Z.Y., Peng, X.Q., Moran, B., 2006. A composites-based hyperelastic constitutive model for soft tissue with application to the human annulus fibrosus. Journal of the Mechanics and Physics of Solids 54, 1952–1971.
Harley, R., James, D., Miller, A., White, J., 1977. Phonons and the elasticn moduli of collagen and muscle. Nature 267, 285–287.
Hofmann, H., Voss, T., Kuhn, K., Engel, J., 1984. Localization of flexible sites in thread-like molecules from electron-micrographs—comparison of interstitial, basement-membrane and intima collagens. Journal of Molecular Biology 172, 325–343.
Holzapfel, G.A., 2000. Nonlinear Solid Mechanics. A Continuum Approach for Engineering. John Wiley & Sons, Chichester, UK.
Holzapfel, G.A., Gasser, T.C., Ogden, R.W., 2000. A new constitutive framework for arterial wall mechanics and a comparative study of material models. Journal of Elasticity 61, 1–48.
Hulmes, D.J.S., 2008. Collagen diversity, synthesis and assembly. In: Fratzl, P. (Ed.), Collagen: Structure and Mechanics. Springer Science, New York, pp. 15–47.
Humphrey, J.D., 2003. Continuum biomechanics of soft biological tissues. Proceedings of the Royal Society A-Mathematical Physical and Engineering Sciences 459, 3–46.
Humphrey, J.D., Yin, F.C.P., 1987. On constitutive relations and finite deformations of passive cardiac tissue. 1. A pseudostrain-energy function. Journal of Biomechanical Engineering, Transactions of the ASME 109, 298–304.
Hurschler, C., Loitz-Ramage, B., Vanderby, R.J., 1997. A structurally based stress–stretch relationship for tendon and ligament. Journal of Biomechanical Engineering 119, 392–399.
Ito, D., Tanaka, E., Yamamoto, S., 2010. A novel constitutive model of skeletal muscle taking into account anisotropic damage. Journal of the Mechanical Behavior of Biomedical Materials 3, 85–93.
Jemec, G.B.E., Serup, J., 1990. Epidermal hydration and skin mechanics. Acta Derm Venereol (Stockh) 70, 245–247; 1990. Acta Dermato-Venereologica 70, 245–247.
Korelc, J., šolinc, U., Wriggers, P., 2010. An improved eas brick element for finite deformation. Computational Mechanics 46, 641–659.
Kramer, R.Z., Venugopal, M.G., Bella, J., Mayville, P., Brodsky, B., Berman, H.M., 2000. Staggered molecular packing in crystals of a collagen-like peptide with a single charged pair. Journal of Molecular Biology 301, 1191–1205.
Kratky, O., Porod, G., 1949. Röntgenuntersuchungen gelöster fadenmoleküle. Recueil des Travaux Chimiques des Pays-Bas et de la Belgique 68, 1106–1122.
Kuhl, E., Garikipati, K., Arruda, E.M., Grosh, K., 2005. Remodeling of biological tissue: mechanically induced reorientation of a transversely isotropic chain network. Journal of the Mechanics and Physics of Solids 53, 1552–1573.
Kuhl, E., Holzapfel, G.A., 2007. A continuum model for remodeling in living structures. Journal of Materials Science 42, 8811–8823.
Kvistedal, Y.A., Nielsen, P.M.F., 2009. Estimating material parameters of human skin in vivo. Biomechanics and Modeling in Mechanobiology 8, 1–8.

Landau, L.D., Lifshitz, E.M., 1986. Theory of Elasticity. Pergamon, Oxford.

Lanir, Y., 1983. Constitutive equations for fibrous connective tissues. Journal of Biomechanics 16, 1–22.

Lanir, Y., Fung, Y.C., 1972. Two-dimensional mechanical properties of rabbit skin—II: experimental results. Journal of Biomechanics 7, 171–182.

Limbert, G., 2009. A stochastic finite element study of the wrinkling behaviour of skin. In: Third International Conference on Mechanics of Biomaterials and Tissues, Clearwater, FL, USA.

Limbert, G., Middleton, J., Laizans, J., Dobelis, M., Knets, I., 2003. A transversely isotropic hyperelastic constitutive model of the PDL. Analytical and computational aspects. Computer Methods in Biomechanics and Biomedical Engineering 6, 337–345.

Limbert, G., Taylor, M., 2002. On the constitutive modeling of biological soft connective tissues. A general theoretical framework and tensors of elasticity for strongly anisotropic fiber-reinforced composites at finite strain. International Journal of Solids and Structures 39, 2343–2358.

Limbert, G., Taylor, M., Middleton, J., 2004. Three-dimensional finite element modelling of the human ACL. Simulation of passive knee flexion with a stressed and stress-free ACL. Journal of Biomechanics 37, 1723–1731.

Lorenzo, A.C., Caffarena, E.R., 2005. Elastic properties, Young's modulus determination and structural stability of the tropocollagen molecule: a computational study by steered molecular dynamics. Journal of Biomechanics 38, 1527–1533.

Lu, J., Zhang, L., 2005. Physically motivated invariant formulation for transversely isotropic hyperelasticity. International Journal of Solids and Structures 42, 6015–6031.

Marko, J.F., Siggia, E.D., 1995. Stretching DNA. Macromolecules 28, 8759–8770.

Marsden, J.E., Hughes, T.J.R., 1994. Mathematical Foundations of Elasticity. Dover, New York.

Ogden, R.W., 1972. Large deformation isotropic elasticity—correlation of theory and experiment for compressible rubberlike solids. Proceedings of the Royal Society of London Series A-Mathematical and Physical Sciences 328, 567.

Ogden, R.W., 1984. Non-Linear Elastic Deformations. Ellis Horwood Ltd., West Sussex, England.

Ogden, R.W., Saccomandi, G., Sgura, I., 2006. On worm-like chain models within the three-dimensional continuum mechanics framework. Proceedings of the Royal Society A—Mathematical Physical and Engineering Sciences 462, 749–768.

Ogden, R.W., Saccomandi, G., Sgura, I., 2007. Computational aspects of worm-like-chain interpolation formulas. Computers & Mathematics with Applications 53, 276–286.

Oomens, C.W.J., Vancampen, D.H., Grootenboer, H.J., 1987. A mixture approach to the mechanics of skin. Journal of Biomechanics 20, 877–885.

Peng, X.Q., Guo, Z.Y., Moran, B., 2006. An anisotropic hyperelastic constitutive model with fiber-matrix shear interaction for the human annulus fibrosus. Journal of Applied Mechanics, Transactions of the ASME 73, 815–824.

Pioletti, D.P., Rakotomanana, L.R., Benvenuti, J.F., Leyvraz, P.F., 1998. Viscoelastic constitutive law in large deformations: application to human knee ligaments and tendons. Journal of Biomechanics 31, 753–757.

Sasaki, N., Odajima, S., 1996a. Stress–strain curve and Young's modulus of a collagen molecule as determined by the X-ray diffraction technique. Journal of Biomechanics 29, 655–658.

Schafer, R.D., 1996. An Introduction to Non-Associative Algebra. Dover Publications, Mineola, NY.

Schröder, J., Neff, P., 2003. Invariant formulation of hyperelastic transverse isotropy based on polyconvex free energy functions. International Journal of Solids and Structures 40, 401–445.

Shimizu, H., 2007. Shimizu's Textbook of Dermatology. Hokkaido University Press, Nakayama Shoten Publishers.

Simo, J.C., Miehe, C., 1992. Associative coupled thermoplasticity at finite strains-formulation, numerical-analysis and implementation. Computer Methods in Applied Mechanics and Engineering 98, 41–104.

Spencer, A.J.M., 1992a. Continuum Theory of the Mechanics of Fibre-Reinforced Composites. Springer-Verlag, New York.

Spencer, A.J.M., 1992b. Plasticity theory for fibre-reinforced composites. Journal of Engineering Mathematics 26, 107–118.

Sun, Y.L., Luo, Z.P., An, K.N., 2001. Stretching short biopolymers using optical tweezers. Biochemical and Biophysical Research Communications 295, 826–830.

Sun, Y.L., Luo, Z.P., Fertala, A., An, K.N., 2002. Direct quantification of the flexibility of type I collagen monomer. Biochemical and Biophysical Research Communications 295, 382–386.

Sun, Y.L., Luo, Z.P., Fertala, A., An, K.N., 2004. Stretching type II collagen with optical tweezers. Journal of Biomechanics 37, 1665–1669.

Tang, Y., Ballarini, R., Buehler, M.J., Eppell, S.J., 2010. Deformation micromechanisms of collagen fibrils under uniaxial tension. Journal of the Royal Society Interface 7, 839–850.

Tang, H., Buehler, M.J., Moran, B., 2009. A constitutive model of soft tissue: from nanoscale collagen to tissue continuum. Annals of Biomedical Engineering 37, 1117–1130.

van der Rijt, J.A.J., van der Werf, K.O., Bennink, M.L., Dijkstra, P.J., Feijen, J., 2006. Micromechanical testing of individual collagen fibrils. Macromolecular Bioscience 6, 697–702.

Vesentini, S., Fitié, C.F.C., Montevecchi, F.M., Redaelli, A., 2005. Molecular assessment of the elastic properties of collagen-like homotrimer sequences. Biomechanics and Modeling in Mechanobiology 3, 224–234.

Wagner, D.R., Lotz, J.C., 2004. Theoretical model and experimental results for the nonlinear elastic behavior of human annulus fibrosus. Journal of Orthopaedic Research 22, 901–909.

Weiss, J.A., Maker, B.N., Govindjee, S., 1996. Finite element implementation of incompressible transversely isotropic hyperelasticity. Computer Methods in Applied Mechanics and Engineering 135, 107–128.